UNH-09-06
JLAB-THY-09-1116
NT@UW-09-26
IUHET-539
ATHENA-PUB-09-019

arXiv:0912.4243v1 [hep-lat] 21 Dec 2009

High Statistics Analysis using Anisotropic Clover Lattices: (III) Baryon-Baryon Interactions

Silas R. Beane,[1] William Detmold,[2,3] Huey-Wen Lin,[4] Thomas C. Luu,[5]
Kostas Orginos,[2,3] Martin J. Savage,[4] Aaron Torok,[6] and André Walker-Loud[2]

(NPLQCD Collaboration)

[1]*Department of Physics, University of New Hampshire, Durham, NH 03824-3568.*
[2]*Department of Physics, College of William and Mary, Williamsburg, VA 23187-8795.*
[3]*Jefferson Laboratory, 12000 Jefferson Avenue, Newport News, VA 23606.*
[4]*Department of Physics, University of Washington, Seattle, WA 98195-1560.*
[5]*N Division, Lawrence Livermore National Laboratory, Livermore, CA 94551.*
[6]*Department of Physics, Indiana University, Bloomington, IN 47405.*

(Dated: December 21, 2009 - 20:51)

Abstract

Low-energy baryon-baryon interactions are calculated in a high-statistics lattice QCD study on a single ensemble of anisotropic clover gauge-field configurations at a pion mass of $m_\pi \sim 390$ MeV, a spatial volume of $L^3 \sim (2.5 \text{ fm})^3$, and a spatial lattice spacing of $b \sim 0.123$ fm. Lüscher's method is used to extract nucleon-nucleon, hyperon-nucleon and hyperon-hyperon scattering phase shifts at one momentum from the one- and two-baryon ground-state energies in the lattice volume. The isospin-3/2 $N\Sigma$ interactions are found to be highly spin-dependent, and the interaction in the ${}^3S_1$ channel is found to be strong. In contrast, the $N\Lambda$ interactions are found to be spin-independent, within the uncertainties of the calculation, consistent with the absence of one-pion-exchange. The only channel for which a negative energy-shift is found is $\Lambda\Lambda$, indicating that the $\Lambda\Lambda$ interaction is attractive, as anticipated from model-dependent discussions regarding the H-dibaryon. The NN scattering lengths are found to be small, clearly indicating the absence of any fine-tuning in the NN-sector at this pion mass. This is consistent with our previous Lattice QCD calculation of NN interactions. The behavior of the signal-to-noise ratio in the baryon-baryon correlation functions, and in the ratio of correlation functions that yields the ground-state energy splitting is explored. In particular, focus is placed on the window of time slices for which the signal-to-noise ratio does not degrade exponentially, as this provides the opportunity to extract quantitative information about multi-baryon systems.

I. INTRODUCTION

The strong interactions among baryons are key to every aspect of our existence. The two- and higher-body interactions among protons and neutrons conspire to produce the spectrum of nuclei and the complicated chains of nuclear reactions that allow for the production of the elements forming the periodic table at the earliest times of our universe, in the stellar environments that follow, and in reactors and our laboratories. Decades of experimental effort have provided a very-precise set of measurements of the nucleon-nucleon scattering cross sections over a wide range of energies [1], and these cross sections have in turn given rise to the modern nuclear forces. These experimentally determined two-body forces, encoded by potentials such as AV_{18} [2] and the chiral potentials [3], when supplemented with three-body interactions, now provide the cornerstone of our theoretical description of nuclei [4] and their interactions. The two-nucleon forces are observed to be significantly more important than the three-nucleon forces, which, in turn, are significantly more important than the four-nucleon forces. Present-day calculations are sufficiently precise that the inclusion of three-nucleon forces is required in order to post-dict the structure of light nuclei [5, 6]. Given the relatively small contributions of the three-nucleon and higher-body interactions to light-nuclei, where reliable calculations are presently possible, there is considerable uncertainty with regard to their form. This leads to enhanced uncertainties in the calculation of systems for which there is little or no experimental guidance, such as moderate to high-density neutron-rich environments, and more generally, nuclear environments at densities exceeding that of nuclear matter.

In dense nuclear systems it is not only the multi-nucleon forces that are difficult to quantify as non-nucleonic objects may play an important role. In a core-collapse supernova, it is the nuclear equation of state (NEOS) that ultimately dictates whether the system collapses into a neutron star or forms a black hole. This, in turn, is determined by the composition and structure of the hadronic matter in the core of the supernova, which is at (baryon number) densities that are a few times that of nuclear matter. At such densities, the strange quark may play a pivotal role through the formation of a charged kaon condensate made possible by the strength of attractive kaon-nucleon interactions. It may also become energetically favorable for the matter to contain strange baryons, such as the Σ^- or Λ, because of their interactions with nucleons. In either case, it is the two-body interactions between the strange hadrons and the nucleons, and also between themselves, that largely determine the composition of the hadronic matter at core-collapse densities, and ultimately the fate of the collapsing supernova [7]. Unfortunately, experimental determinations of the interactions of strange hadrons are very challenging due to their weak decays, and existing cross-section measurements are not precise enough to provide meaningful constraints on the NEOS at core-collapse densities. So, while it is the interactions between three-nucleons that currently limit the precision with which properties of material composed of neutrons and protons can be calculated, it is the two-body interactions involving strange hadrons that currently provide the most serious limitation to reliable calculations at densities that exceed that of nuclear matter.

One of the major objectives of lattice QCD (LQCD) is to calculate the properties and interactions of nucleons and, more generally, systems comprised of multiple hadrons. Precise exploration of the simplest multi-hadron systems has recently become possible with significant advances in computational resources, as well as through algorithmic and theoretical developments (for a recent review, see Ref [8]). The $I = 2$ two-pion system, $\pi^+\pi^+$, is the simplest of such multi-hadron systems to calculate in LQCD, and current computational resources have allowed for a $\sim 1\%$ level determination of the $\pi^+\pi^+$ scattering length [9, 10, 11]. Further, systems comprised of up to twelve π^+'s [12, 13] and systems comprised of up to twelve K^+'s [14] have been explored, allowing a determination of the three-π^+ and three-K^+ interactions as well as aspects of pion and kaon condensates.

In general, a determination of the two-particle scattering amplitude, or multi-body interactions, with LQCD requires calculating the energy eigenvalues of the appropriate two-hadron system in the finite volume [15, 16, 17]. The energy differences between the multi-particle energy levels in the finite volume and the sum of the particle masses determines the scattering amplitude at the corresponding energy. Processes of interest to low-energy nuclear physics occur in the MeV energy regime, while the masses of the baryons and nuclei are in the GeV regime. As a result, very precise (high-statistics) measurements must be performed in order to reliably extract useful constraints on two- and higher-body interactions from a lattice calculation.

In contrast to mesonic systems, lattice QCD calculations in the baryon sector are complicated by the statistical behavior of the correlation functions [18]. We performed the first unquenched LQCD calculation of nucleon-nucleon (NN) [19] and hyperon-nucleon (YN) [20] scattering lengths, and found that the NN scattering lengths appear to be of natural size at larger pion masses, and are set by the range of the interaction. Consequently, an increase in the magnitude of the scattering length as the pion mass is reduced down to its physical value is anticipated. Further, we have recently performed the first lattice QCD calculation of scattering in various meson-baryon channels [21] using the mixed-action scheme of domain-wall valence quarks on the MILC staggered sea.

Recently, we have performed a high-statistics calculation of a number of single-hadron correlation functions [22] and also the first calculations of three-baryon systems [23] on an ensemble of the anisotropic gauge-field configurations generated by the Hadron Spectrum Collaboration [24, 25]. This ensemble has a pion mass of $m_\pi \sim 390$ MeV, a spatial lattice spacing of $b_s = 0.1227 \pm 0.0008$ fm, an anisotropy $\xi = b_s/b_t = 3.500 \pm 0.032$ and a lattice volume of $L^3 \times T = 20^3 \times 128$. The goal of those studies was to "jump" an order of magnitude in the number of measurements performed to estimate correlation functions, and to explore the "new territory" that subsequently emerged. The baryon masses were extracted with fully quantified uncertainties at the $\lesssim 0.2\%$-level from the 0.28×10^6 measurements performed on 1194 gauge-field configurations. With a somewhat smaller statistical sample, the binding energies of the pnn (triton $\equiv {}^3$He by the isospin symmetry of the LQCD calculation) and "$\Xi^0\Xi^0 n$" three-baryon systems were investigated and in the latter case, determined with an uncertainty of ~ 3 MeV/baryon. Subsequently, a study of the ^{3}He (ppn) and ^{4}He ($ppnn$) systems in quenched QCD at a large quark mass appeared [26]. A number of important and surprising observations were made in those works [22, 23, 26] that have modified how we foresee moving toward calculating the properties of light nuclei.

One of the most important aspects of our previous work was the detailed study of the signal-to-noise ratio in the single-baryon correlation functions. The signal-to-noise ratio was found to be approximately independent of time for a significant number of time-slices [22, 23] prior to evolving toward the expected exponential degradation [18]. This window of time-slices is understood in terms of the suppression of contributions from purely mesonic states in the correlation function that determines the variance of the single-baryon correlation function. Given that the signal-to-noise ratio for a system containing more than one baryon is expected to scale (approximately) as the product of the signal-to-noise ratio's of the individual baryons (neglecting their interactions), this window of time slices suggests that calculations of the energy levels of systems containing a number of baryons in this lattice volume with these interpolating operators is possible. In this work we present the baryon-baryon scattering phase shifts that have been measured in our high-statistics anisotropic clover-quark calculation.

Our analysis and results are presented in the following manner. In Section II, we introduce the details of the formalism used in extracting phase shifts from our LQCD calculations. Section III briefly reviews our single baryon results before we present our extractions of two-baryon interactions in Section IV. Section V details our analysis of statistical scaling and noise in the various correlation functions while Section VI is a concluding discussion.

II. LATTICE QCD CALCULATIONS

A. Lüscher method for extracting scattering parameters

In this work, the finite volume scaling method (Lüscher's method) [15, 16, 17] is employed to extract the two-particle scattering amplitudes below inelastic thresholds at a given energy. In the situation where only a single scattering channel is kinematically allowed, the deviation of the energy eigenvalues of the two-hadron system in the lattice volume from the sum of the single-hadron masses is related to the scattering phase shift, δ. For energy eigenvalues above kinematic thresholds where multiple channels contribute, a coupled-channels analysis is required as a single phase shift does not parameterize the S-matrix. The energy shift for two particles A and B, $\Delta E = E_{AB} - E_A - E_B$, can be determined from the correlation functions for systems containing one and two hadrons. For baryon-baryon systems, correlation functions of the form

$$\begin{aligned} C_{\mathcal{B};\Gamma}(\mathbf{p},t) &= \sum_{\mathbf{x}} e^{i\mathbf{p}\cdot\mathbf{x}}\ \Gamma_{\alpha}^{\beta}\ \langle \mathcal{B}_\alpha(\mathbf{x},t)\ \overline{\mathcal{B}}_\beta(\mathbf{x}_0,0)\rangle \\ C_{\mathcal{B}_1,\mathcal{B}_2;\Gamma}(\mathbf{p}_1,\mathbf{p}_2,t) &= \sum_{\mathbf{x}_1,\mathbf{x}_2} e^{i\mathbf{p}_1\cdot\mathbf{x}_1} e^{i\mathbf{p}_2\cdot\mathbf{x}_2}\Gamma_{\beta_1\beta_2}^{\alpha_1\alpha_2}\langle \mathcal{B}_{1,\alpha_1}(\mathbf{x}_1,t)\mathcal{B}_{2,\alpha_2}(\mathbf{x}_2,t)\overline{\mathcal{B}}_{1,\beta_1}(\mathbf{x}_0,0)\overline{\mathcal{B}}_{2,\beta_2}(\mathbf{x}_0,0)\rangle\ , \end{aligned} \tag{1}$$

are used, where $\mathcal{B}$ denotes a baryon interpolating operator, $\alpha_{(i)}$ and $\beta_{(i)}$ are Dirac indices, and the Γ are spin tensors that typically project onto particular parity and/or angular momentum states. The baryon octet interpolating operators are of the form

$$\begin{aligned} p_\alpha(\mathbf{x},t) &= \epsilon^{ijk} u^i_\alpha(\mathbf{x},t)\left(u^{j\mathsf{T}}(\mathbf{x},t)C\gamma_5 d^k(\mathbf{x},t)\right)\ , \\ \Lambda_\alpha(\mathbf{x},t) &= \epsilon^{ijk} s^i_\alpha(\mathbf{x},t)\left(u^{j\mathsf{T}}(\mathbf{x},t)C\gamma_5 d^k(\mathbf{x},t)\right)\ , \\ \Sigma^+_\alpha(\mathbf{x},t) &= \epsilon^{ijk} u^i_\alpha(\mathbf{x},t)\left(u^{j\mathsf{T}}(\mathbf{x},t)C\gamma_5 s^k(\mathbf{x},t)\right)\ , \\ \Xi^0_\alpha(\mathbf{x},t) &= \epsilon^{ijk} s^i_\alpha(\mathbf{x},t)\left(u^{j\mathsf{T}}(\mathbf{x},t)C\gamma_5 s^k(\mathbf{x},t)\right)\ , \end{aligned} \tag{2}$$

where C is the charge-conjugation matrix and ijk are color indices. Other hadrons in the lowest-lying octet can be obtained from the appropriate combinations of quark flavors. The parentheses in the interpolating operators indicate contraction of spin indices into a spin-0 "diquark". It is worth pointing out that the overlap of the composite operator $\mathcal{B}_{1,\alpha_1}(\mathbf{x}_1,t)\mathcal{B}_{2,\alpha_2}(\mathbf{x}_2,t)$ onto two-baryon states is not simply the product of individual baryon "Z-factors", but depends explicitly upon $\mathbf{x}_1-\mathbf{x}_2$, with a correlation length set by the pion mass. This fact precludes a determination of interpolator-independent baryon-baryon potentials from lattice QCD calculations [27].

Away from the time slice on which the source is placed (in this case $t = 0$) these correlation functions behave as

$$C_{\mathcal{H}_A}(\mathbf{p}, t) \ = \ \sum_n \ Z^{(i)}_{n;A}(\mathbf{p}) \ Z^{(f)}_{n;A}(\mathbf{p}) \ e^{-E^{(A)}_n(\mathbf{p}) \ t} \ , \tag{3}$$

$$C_{\mathcal{H}_A\mathcal{H}_B}(\mathbf{p}, -\mathbf{p}, t) \ = \ \sum_n \ Z^{(i)}_{n;AB}(\mathbf{p}) \ Z^{(f)}_{n;AB}(\mathbf{p}) \ e^{-E^{(AB)}_n(\mathbf{0}) \ t} \ , \tag{4}$$

with $E^{(A)}_0(\mathbf{0}) = m_A$ and the $E^{(AB)}_n(\mathbf{0})$ are the energy-eigenvalues of the two particle system (we only present calculations of two-baryon systems for which the center-of-mass is at rest) in the lattice volume. At large times, the ratio

$$\frac{C_{\mathcal{H}_A\mathcal{H}_B}(\mathbf{p}, -\mathbf{p}, t)}{C_{\mathcal{H}_A}(\mathbf{0}, t) C_{\mathcal{H}_B}(\mathbf{0}, t)} \ \overset{t\rightarrow\infty}{\longrightarrow} \ \widetilde{Z}^{(i)}_{0,AB}(\mathbf{p}) \widetilde{Z}^{(f)}_{0,AB}(\mathbf{p}) \ e^{-\Delta E^{(AB)}_0(\mathbf{0}) \ t} \tag{5}$$

decays as a single exponential in time with the energy shift, $\Delta E^{(AB)}_0(\mathbf{0})$. In what follows, only the case $\mathbf{p} = \mathbf{0}$ is considered. The energy shifts

$$\begin{aligned} \Delta E^{(AB)}_n \equiv \Delta E^{(AB)}_n(\mathbf{0}) \ &\equiv \ E^{(AB)}_n(\mathbf{0}) - m_A - m_B = \sqrt{q_n^2 + m_A^2} + \sqrt{q_n^2 + m_B^2} - m_A - m_B \\ &= \ \frac{q_n^2}{2\mu_{AB}} + \ldots \ , \end{aligned} \tag{6}$$

(where $\mu_{AB} = m_A m_B/(m_A + m_B)$ is the reduced mass of the two-particle system) determine squared momenta, q_n^2 (which can be either positive or negative). Below inelastic thresholds, these are related to the real part of the inverse scattering amplitude via [1]

$$q_n \ \cot\delta(q_n) = \frac{1}{\pi \ L} S\left(q_n^2 \left(\frac{L}{2\pi}\right)^2\right) \ , \tag{8}$$

where

$$S(x) = \lim_{\Lambda\rightarrow\infty} \sum_{\mathbf{j}}^{|\mathbf{j}|<\Lambda} \frac{1}{|\mathbf{j}|^2 - x} - 4\pi \ \Lambda \, , \tag{9}$$

thereby implicitly determining the value of the phase shift at the energy $\Delta E^{(AB)}_n$ (or center of mass momentum q_n), $\delta(q_n)$. Thus, the function $p\cot\delta(p)$, that determines the low-energy

---

[1] Calculations performed on anisotropic lattices, such as those used in this work, require a modified energy-momentum relation, and as a result eq. (6) becomes

$$\Delta E^{(AB)}_n \ \equiv \ E^{(AB)}_n - m_A - m_B = \sqrt{q_n^2/\xi_A^2 + m_A^2} + \sqrt{q_n^2/\xi_B^2 + m_B^2} - m_A - m_B \ \ , \tag{7}$$

where $\xi_{A,B}$ are the anisotropy factors for particle A and particle B, respectively, determined from the appropriate energy-momentum dispersion relation. The masses and energy splitting are given in terms of temporal lattice units and q_n is given in spatial lattice units. In the present work we find that the various ξ_A agree within uncertainties and have used $\xi_A = \xi_B = \xi$ for all scattering processes.

elastic-scattering cross-section, $\mathcal{A}(p) \propto (p\cot\delta(p) - i\,p)^{-1}$, is determined at the energy $\Delta E_n^{(AB)}$.

For a scattering process for which the exchange of a single pion (One-Pion-Exchange (OPE)) is allowed by spin and isospin considerations, the function $p\cot\delta(p)$ is a analytic function of $|\mathbf{p}|^2$ for $|\mathbf{p}| \leq m_\pi/2$ (determined by the t-channel cut in the scattering amplitude). In this kinematic regime, $p\cot\delta(p)$ has a series-expansion (the effective range expansion) of the form

$$p\cot\delta(p) \;=\; -\frac{1}{a} \;+\; \frac{1}{2}\, r_0\, |\mathbf{p}|^2 \;+\; ... \quad , \tag{10}$$

where a is the scattering length (with the nuclear physics sign convention) and r_0 is the effective range. While the magnitude of the effective range (and higher terms) is set by the pion mass, the scattering length is unconstrained. For scattering processes where OPE is not allowed, the lower limit of the cut in the t-channel and the location of inelastic threshold set the radius of convergence of the effective-range expansion of $p\cot\delta(p)$.

B. Expectations at finite temporal extent

For baryon-baryon correlation functions computed from quark propagators that are anti-periodic in the time direction, and using the sources of eq. (2), the correlation functions contain contributions from hadronic states propagating forwards and backwards in time. They are expected to have the form

$$\begin{aligned} C_{\mathcal{B}\mathcal{B};\Gamma_+}(\mathbf{0},\mathbf{0},t) \;=\; & Z_1\; e^{-E_{\mathcal{B}\mathcal{B}}t} \;+\; Z_2\; e^{-E_{\mathcal{B}'\mathcal{B}'}(T-t)} \;+\; Z_3\; e^{-E_{\mathcal{B}}t} e^{-E_{\mathcal{B}'}(T-t)} \\ & +\; Z_4\; e^{-E_{\mathcal{B}\mathcal{B}}(T-t)} + Z_5\; e^{-E_{\mathcal{B}'\mathcal{B}'}t} \;+\; \ldots\,, \end{aligned} \tag{11}$$

where $E_{\mathcal{B}\mathcal{B}}$ is the energy of the two-baryon state, $E_{\mathcal{B}}$ is the ground-state baryon energy of positive parity, $E_{\mathcal{B}'}$ is the energy of the ground-state negative-parity baryon or meson-baryon scattering state and the ellipsis denotes contributions from higher excited states of the same quantum numbers. The exponent of the first term in eq. (11) is the primary object of our study and the other contributions are viewed as "pollutants".

Since the interpolating operators for the baryons that give rise to the baryon-baryon correlation functions are individually projected with the positive-energy projectors, $\Gamma_\pm = (1\pm\gamma_0)/2$, the Z-factors of the forward and backward propagating states of the same energy in eq. (11) are not related, for example it is possible that $Z_4 \neq Z_1$. Indeed, since the sink separately projects the parity of each baryon (along with its momentum), the amplitude of the two backwards propagating baryons is suppressed by the lattice volume relative to the two forwards propagating baryons. This is a significant suppression, and we expect to see more energetic states, such as $\mathcal{B}'\mathcal{B}'$, dominating the correlation function at large times near the boundary.

C. Computational overview

In the present study, we have employed a single ensemble of $20^3 \times 128$ gauge-field configurations generated with a $n_f = 2+1$ flavor, anisotropic-clover quark action, with a spatial lattice spacing of $b = 0.1227(8)$ fm and a pion mass $m_\pi \sim 390$ MeV, that have been produced by the Hadron Spectrum Collaboration [24, 25]. The technical details of the propagators computed on this ensemble are presented in Ref. [22] and we do not repeat them here. In the current calculation, the number of measurements has been increased to an average of 364 randomly-distributed measurements on each of 1195 configurations (a total of $\sim 0.435 \times 10^6$ measurements). For correlators from each source point, two types of sink interpolating operators are used [22] and the resulting correlation functions are referred to as "smeared-point" (SP) and "smeared-smeared" (SS). The measurements on each configuration are averaged, and then these averaged measurements are typically blocked (averaged) in sets of ten neighboring configurations (100 trajectories) to account for residual correlations (see Ref. [22] for a detailed study of correlations between different sources and configurations).

The methods used to determine quantities of interest from the measured correlation functions are discussed in detail in Refs. [22, 23], and we present no more than an overview here. One method of extraction is a direct analysis of "effective plots". Linear combinations of the SP and SS correlation functions associated with each baryon and baryon-baryon state are formed to eliminate the contribution from excited states, as discussed in Ref. [22]. Effective mass plots are formed from these correlation functions and ratios of correlation functions to extract the energy and energy splitting, respectively[2]. Time intervals over which the effective mass appears constant are identified, and the energy is extracted from a correlated χ^2-squared minimization with the covariance matrix determined with the Jackknife or Bootstrap procedure. A fitting systematic uncertainty is assigned from the range of extracted energies determined by varying the location and size of the fitting interval over a reasonable range. A given energy-splitting and its uncertainty is converted into a value of q_n^2 and its uncertainty using eq. (6), or a direct fit to an effective-q_n^2 plot is performed, which is then translated into $q_n \cot\delta(q_n)$ and its associated uncertainty using eq. (8). There are a number of ways to perform this last stage of the analysis. One way is to use the Jackknife or Bootstrap procedure to determine the uncertainty in $q_n \cot\delta(q_n)$ directly. However, this is complicated by the fact that $S(x)$ in eq. (8) is a singular function. An alternate method is to determine the value of q_n^2 and its associated uncertainty from the two-baryon energy splitting from eq. (6), and then to propagate the central value and uncertainties through eq. (8) to determine $q_n \cot\delta(q_n)$. We present results using the latter method.

Results from this methodology are consistent with those from multi-exponential fits to the correlation functions and with various matrix-Prony [23] based analyses. In the following, we present results from a single analysis, ensuring that the systematic uncertainties are sufficient to maintain agreement with analyses using these other methods.

---

[2] Linear combination of SP and SS correlation functions are formed that extend the plateau of the ground state found from a matrix-Prony analysis [23] to earlier times. The effect of choosing a slightly different linear combination is taken into account by the systematic error. While we find that the best candidate for the ground state level is not ambiguous in any of the two-baryon correlation functions, there is always the possibility that the "true" ground state becomes dominant in the region where it is likely that there are significant contributions from backward-propagating states which contaminate the signal. Eliminating this possibility requires better statistical precision and/or measurements on lattices with a longer time extent.

III. SINGLE BARYONS

The interaction between baryons is extracted from the difference between the energy-levels of the two baryon system in the lattice volume and the individual baryon masses. The masses of the baryons were extracted in a previous work [22], but it is useful to show the masses here, particularly due to the substantial increase in the number of measurements that have been performed. The baryon masses are extracted from correlated χ^2 minimizing fits to the generalized effective mass plots (GEMP's) obtained from each correlation function, $C_i(t)$, defined to be

$$M_{\mathrm{eff;t_J}}(t) \;=\; \frac{1}{t_J}\;\log\left(\frac{C(t)}{C(t+t_J)}\right) \quad . \tag{12}$$

The GEMP's from the single-baryon correlation functions are presented in fig. 1. The extracted baryon masses that are fit to the plateau regions of the GEMP's are shown along with the statistical uncertainty, and the systematic and statistical uncertainties combined in quadrature. The results of the fitting, along with the fitting intervals are given in Table I.

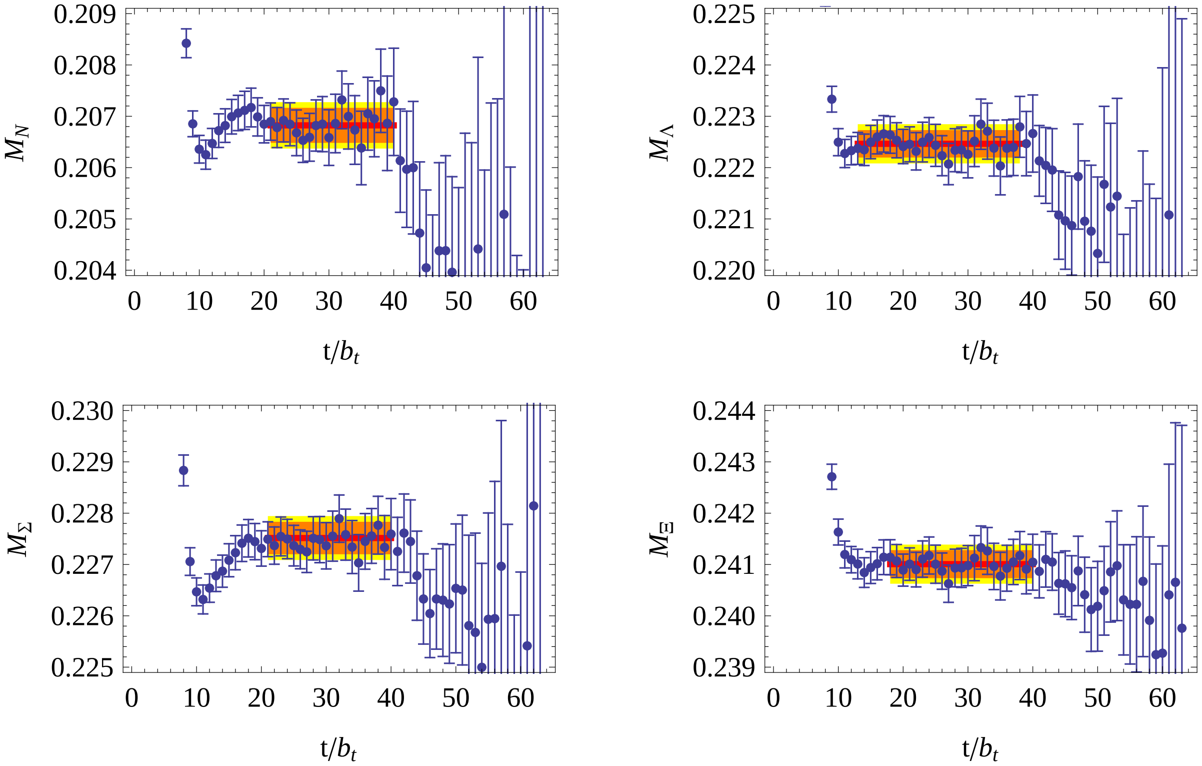

FIG. 1: The single-baryon GEMP's (with $t_J = 3$) resulting from the linear combination of SS and SP correlation functions that eliminates contributions from excited states. The fit values of the masses along with the statistical uncertainty, and the systematic and statistical uncertainties combined in quadrature, are shown.

The statistical and fitting systematic uncertainties are below 0.2% for each of the single baryon states (although the uncertainty in the temporal lattice spacing leads to a larger uncertainty on the masses in physical units). The baryon signal-to-noise ratio is essentially independent of time in the fitting windows shown in Table I due to the nature of the sources

TABLE I: Extracted single hadron masses. A lattice spacing of $b_s = 0.1227 \pm 0.0008$ fm and an anisotropy factor of $\xi_s = 3.500 \pm 0.032$ is used to convert from temporal lattice units (t.l.u.) to MeV. The first two uncertainties are the statistical and systematic uncertainty of the extraction in temporal lattice units, while the third uncertainty quoted for quantities in physical units is the combined lattice spacing and anisotropy uncertainty.

Hadron	M (t.l.u.)	M (MeV)	χ/dof	fitting interval
π	0.06936(12)(05)	390.39(0.67)(0.28)(4.38)	0.73	21 → 41
K	0.097016(99)(33)	546.06(0.56)(0.19)(6.13)	1.01	29 → 49
N	0.20682(34)(30)	1164.1(1.9)(1.7)(13.1)	1.16	21 → 40
Λ	0.22246(27)(27)	1252.1(1.5)(1.5)(14.1)	0.97	13 → 38
Σ	0.22752(32)(29)	1280.6(1.7)(1.6)(14.3)	1.46	21 → 40
Ξ	0.24101(27)(27)	1356.5(1.5)(1.5)(15.2)	1.06	16 → 40

that generate the correlation function, as discussed in Ref. [22]. It is only in these time intervals (for this value of t_J) that reliable energy splittings between the two-baryon and the single-baryon masses can be constructed from the ratio of the correlation functions given in eq. (5).

IV. BARYON-BARYON INTERACTIONS

The energy eigenstates in the finite lattice volume are classified by their global quantum numbers: baryon number, isospin, third component of isospin, strangeness, total momentum, and behavior under hyper-cubic transformations. Six quark operators that are simple products of three-quark baryon operators are used as sources for the baryon-baryon correlation functions. As a consequence, the baryon content of the interpolating operator is used to define the operator, e.g. $n\Lambda(^3S_1)$, but this operator will, in principle, couple to all states in the volume with the quantum numbers $B = 2$, $I = \frac{1}{2}$, $I_z = -\frac{1}{2}$, $s = -1$, and $^{2s+1}L_J = {}^3S_1 + ...$, where the ellipses denote states with higher total angular momentum that also project onto the A_1 irreducible representation of the cubic-group [3]. Both SS and SP correlation functions have been calculated for the nine baryon-baryon channels shown in Table II.

If the calculations were performed on gauge-field configurations of infinite extent in the time-direction, so that only forward propagation could occur, some of the channels in Table II could be analyzed by considering contributions from a single scattering channel, e.g. NN, $\Xi^-\Xi^-$, $\Sigma^-\Sigma^-$, $n\Sigma^-$, as we expect a single, well-separated ground state for these quantum numbers. However, other channels may require a multi-channel analysis, e.g. $n\Lambda$, $\Lambda\Lambda$. The $n\Lambda$ source will produce low-lying states in the lattice volume that are predominately linear

---

[3] The spatial dimensions of the gauge-field configurations that are used in this work are identical (i.e. isotropic), and as such the eigenstates of the QCD Hamiltonian can be classified with respect to their transformation properties under cubic transformations, $H(3)$, a subgroup of the group of continuous three-dimensional rotations, $O(3)$. The two-baryon states that are calculated in this work all belong to the A_1^+ representation of $H(3)$, corresponding to combinations of states with angular momentum $L = 0, 4, 6, \ldots$.

TABLE II: Baryon-baryon channels examined in this work.

Channel	I	$\lvert I_z\rvert$	s
$pp\ (^1S_0)$	1	1	0
$np\ (^3S_1)$	0	0	0
$n\Lambda\ (^1S_0)$	$\frac{1}{2}$	$\frac{1}{2}$	-1
$n\Lambda\ (^3S_1)$	$\frac{1}{2}$	$\frac{1}{2}$	-1
$n\Sigma^-\ (^1S_0)$	$\frac{3}{2}$	$\frac{3}{2}$	-1
$n\Sigma^-\ (^3S_1)$	$\frac{3}{2}$	$\frac{3}{2}$	-1
$\Sigma^-\Sigma^-\ (^1S_0)$	2	2	-2
$\Lambda\Lambda\ (^1S_0)$	0	0	-2
$\Xi^-\Xi^-\ (^1S_0)$	1	1	-4

combinations of the $n\Lambda$, $n\Sigma^0$ and $p\Sigma^-$ two-baryon states. The $\Lambda\Lambda$ source will produce low-lying states in the lattice volume that are predominately linear combinations of the $\Lambda\Lambda$, $\Sigma^{\pm,0}\Sigma^{\mp,0}$, and $N\Xi$ two-baryon states.

A. Nucleon-nucleon interactions

Perhaps the most studied and best understood of the two-hadron systems are the proton-proton and proton-neutron. At low energies, only two combinations of spin and isospin are possible, a spin-triplet isosinglet $np\ (^3S_1)$ and a spin-singlet isotriplet $pp\ (^1S_0)$. At the physical pion mass, the scattering lengths in these channels are unnaturally large and the $^3S_1$ channel contains a shallow bound state, the deuteron, with a binding energy of ~ 2.22 MeV. These large scattering lengths and the shallow bound state arise because the coefficient of the momentum-independent four-nucleon operator in the low-energy effective field theory has a non-trivial ultraviolet fixed-point for the physical light-quark masses. An interesting line of investigation is the study of the scattering lengths as a function of the quark masses to ascertain the sensitivity of this fine-tuning to the QCD parameters [30, 31, 32]. The fine tuning is not expected to persist away from the physical masses and we expect our present (unphysical) calculations to yield scattering lengths that are natural-sized.

The GEMP obtained from the proton-proton correlation functions is shown in fig. 2, and fig. 3 shows the analogous plots for the neutron-proton correlation function. After the initial plateau region, the GEMPs show a slight downward fluctuation at time-slice ~ 29, which we believe is statistical in nature.[4] Figure 4 shows the effective $|\mathbf{k}|^2$ plot [5] for both the proton-proton and neutron-proton channels. Both channels exhibit plateaus in $|\mathbf{k}|^2$. The plateau in the neutron-proton channel is consistent with zero, while the plateau in the proton-proton channel differs from zero at the $\sim 1\sigma$-level. We conclude that at this value of the pion

---

[4] This fluctuation appears in both the proton-proton and neutron-proton GEMPs and in several of the other channels. The fact that the feature appears in multiple correlation functions is not a surprise as all the correlation functions are generated from the same light-quark and strange-quark propagators.

[5] For the presentation of the results of the calculation we use $|\mathbf{k}|^2$ to denote q_n^2, as the GEMPs do not isolate a particular energy-eigenvalue or eigenstate.

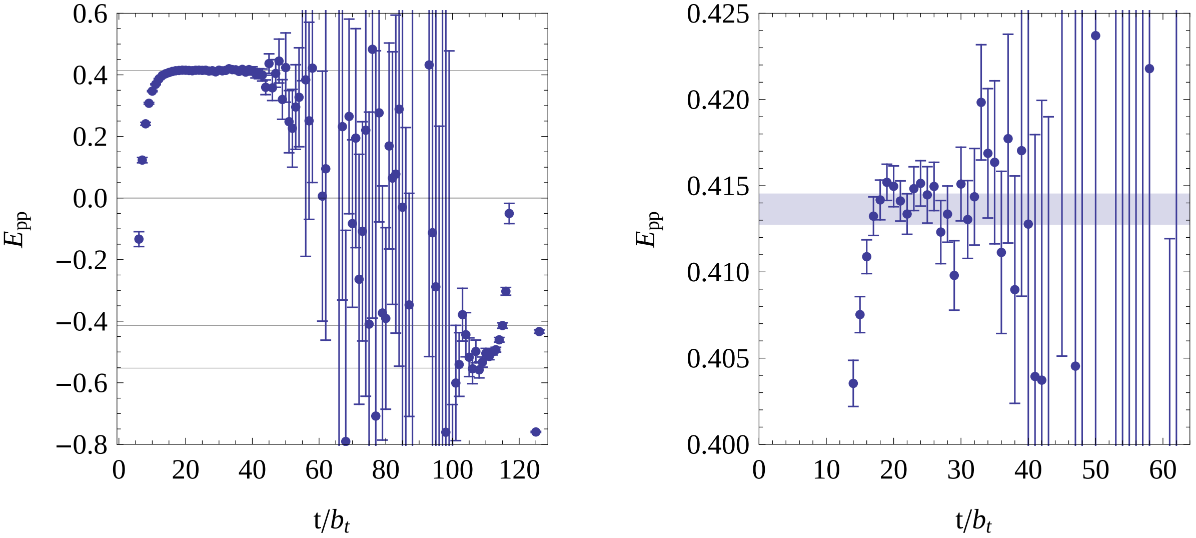

FIG. 2: The left panel is the proton-proton ($^1S_0$) GEMP with $t_J = 1$, while the right panel shows the plateau region of the left panel. The band in the right panel and the upper line in the left panel correspond to $2M_N$, while the lower two lines in the left panel correspond to $-2M_N$ and $-2(M_N + m_\pi)$, respectively.

mass, the interactions between nucleons produce a small scattering length in both channels compared to the naive estimate of $m_\pi^{-1} \sim 0.5$ fm. The results of the analysis are shown in Table III. Extracted lattice quantities are converted to physical units using $b_s = 0.1227(8)$ fm; here the lattice spacing uncertainty is sub-dominant. Motivated by the fact that the pion mass dictates the range of the interaction between nucleons, we have shown $m_\pi/p\cot\delta(p)$ as a function of $|\mathbf{k}|^2/m_\pi^2$ in fig. 5.

TABLE III: Results for the pp ($^1S_0$) and np ($^3S_1$) channels.

Process	$\lvert\mathbf{k}\rvert^2/m_\pi^2$	ΔE (MeV)	$-1/p\cot\delta$ (fm)	χ^2/dof	fitting interval
pp	0.030(13)(20)	3.9(1.7)(2.6)	$0.118^{+0.044}_{-0.049}{}^{+0.065}_{-0.077}$	1.6	20 → 32
np	0.012(20)(33)	1.6(2.6)(4.3)	$0.052^{+0.07}_{-0.09}{}^{+0.11}_{-0.15}$	1.96	19 → 32

A summary of lattice QCD calculations of NN scattering is shown in fig. 6. Since the momenta at which the phase shifts are measured are small, we present these results as scattering lengths, implicitly assuming that higher order coefficients in the effective range expansion, eq. (10), are natural sized. The results calculated in this work are consistent with those that we obtained using mixed-action lattice QCD [19]. It is interesting to note that the results of quenched calculations [29] yield scattering lengths that are consistent within

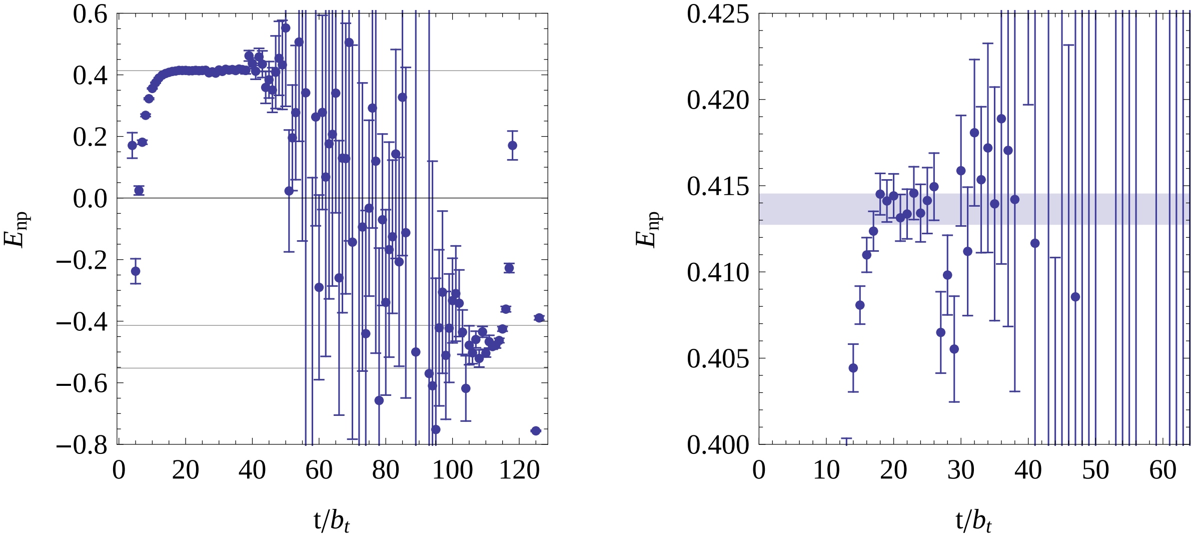

FIG. 3: The left panel is the neutron-proton ($^3S_1$) GEMP with $t_J = 1$, while the right panel shows the plateau region of the left panel. The band in the right panel and the upper line in the left panel correspond to $2M_N$, while the lower two lines in the left panel correspond to $-2M_N$ and $-2(M_N + m_\pi)$, respectively.

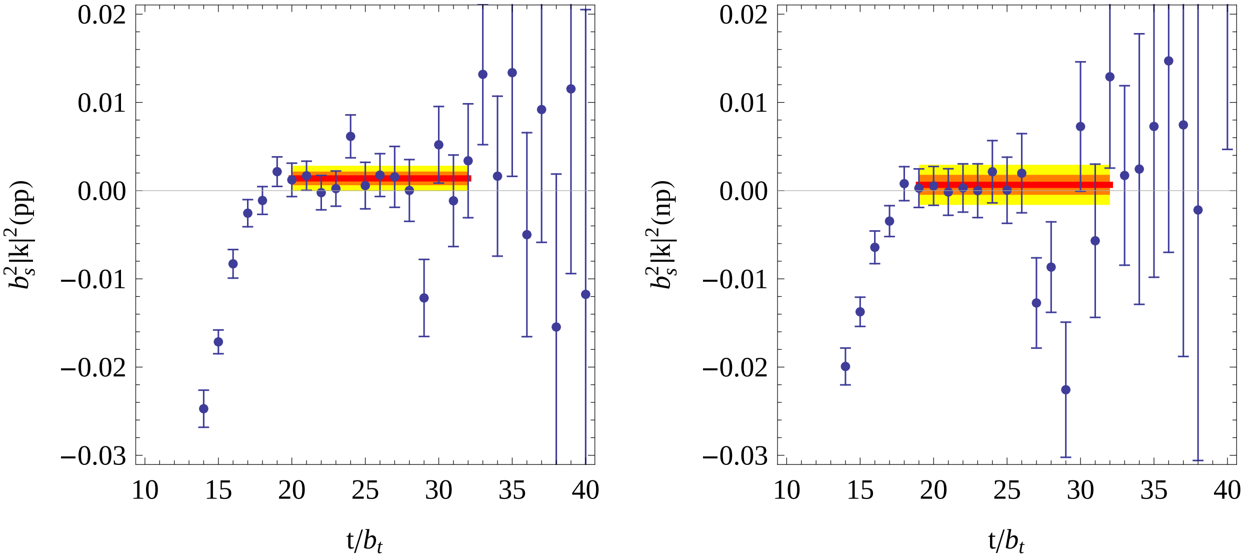

FIG. 4: The left panel is the effective $|\mathbf{k}|^2$ plot for the proton-proton ($^1S_0$) channel with $t_J = 1$ and the fit to the plateau. The right panel is for the neutron-proton ($^3S_1$) channel.

uncertainties with the fully-dynamical $n_f = 2 + 1$ values.

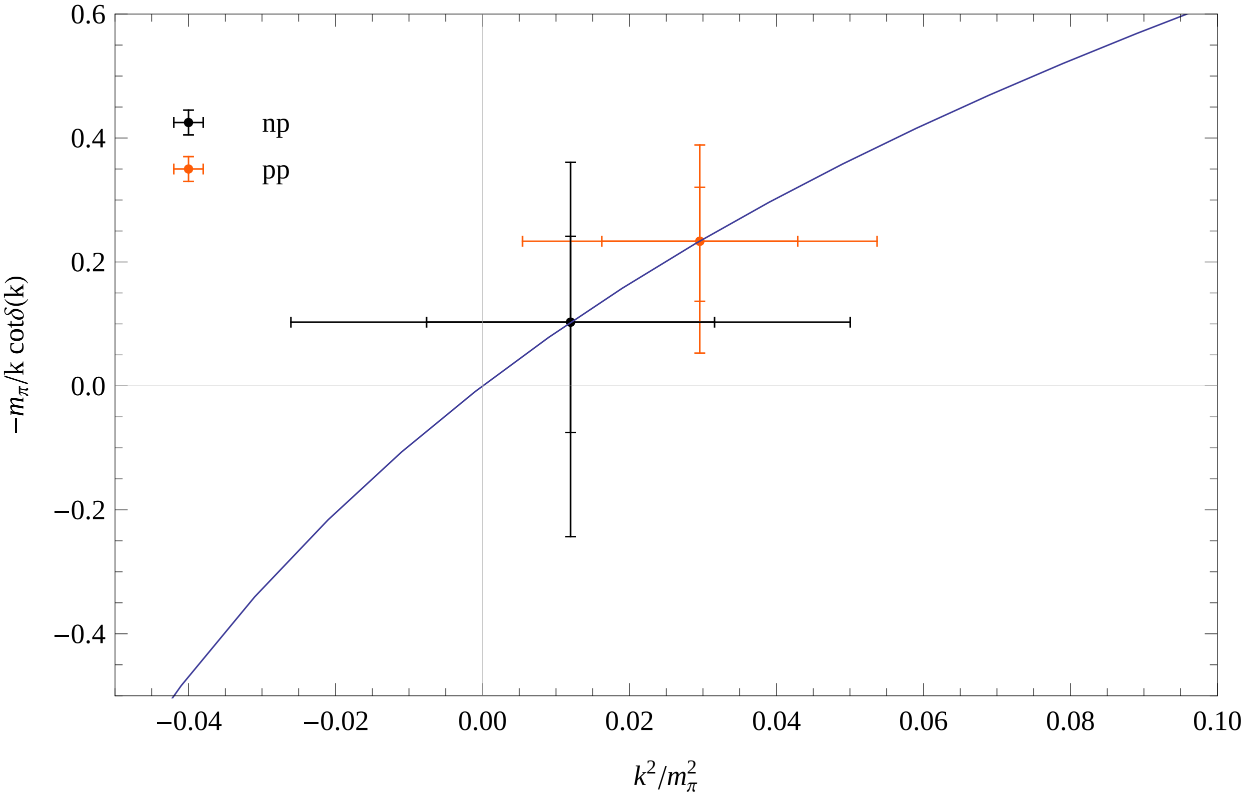

FIG. 5: The inverse of the real part of the inverse scattering amplitude normalized to the pion mass as a function of the squared-momentum in the center-of-mass normalized to the pion mass. The dotted curve corresponds to the inverse "S-function", defined in eq. (8), from which $(k\cot\delta)^{-1}$ is determined from $|\mathbf{k}|^2$. The inner uncertainty of each data point is statistical and the outer uncertainty is the statistical and systematic uncertainty combined in quadrature.

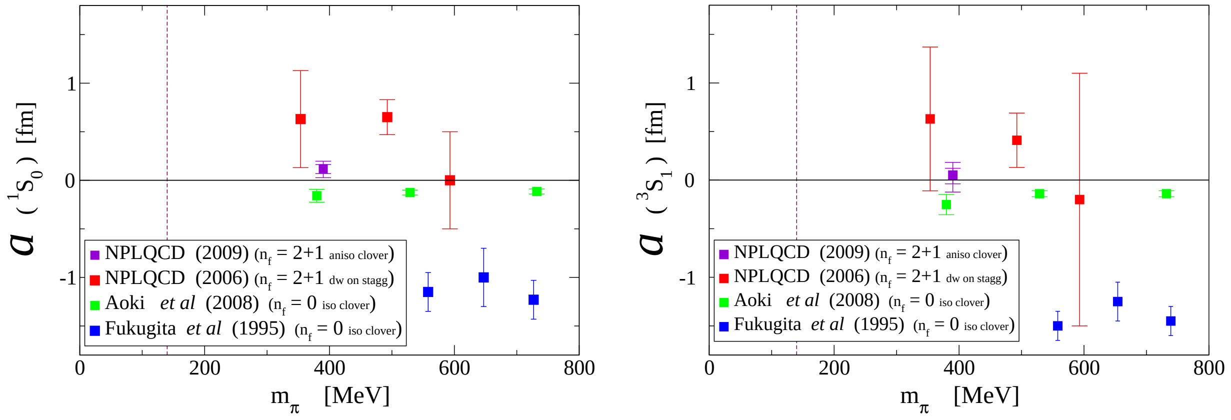

FIG. 6: A compilation of the scattering lengths for NN scattering in the $^1S_0$ (left panel) and $^3S_1$ (right panel) calculated in lattice QCD and quenched lattice QCD. The data are from Refs. [28], [19], [29] and the current work. The vertical dashed line corresponds to the physical pion mass.

B. Hyperon-nucleon interactions ($s = -1$)

Lattice QCD calculations of the YN interactions are of greater phenomenological importance than those of NN interactions because of the limited experimental access to hyperon systems in the laboratory and the possible role of hyperons in nuclear astrophysics. We have calculated the energy-eigenvalues of systems with the quantum numbers of $n\Lambda$ and $n\Sigma^-$ in both spin channels.

1. $n\Sigma^-$ *interactions* ($I = \frac{3}{2}$)

Interpolating operators with the quantum numbers of $n\Sigma^-$ in either the ${}^1S_0$ or ${}^3S_1$ channels will couple to energy eigenstates in the lattice volume with strangeness $s = -1$ and isospin of $I = \frac{3}{2}$, and the spectrum is not expected to have more than one low-lying ground state. We expect to be able to describe these systems with a single elastic-scattering channel for the lattice volumes we are working in as these are the only two-baryon states comprised of octet baryons that have these quantum numbers.

The GEMP for the $n\Sigma^-$ (${}^1S_0$) is shown in fig. 7 and exhibits a clear plateau, as does the GEMP for the $n\Sigma^-$ (${}^3S_1$) channel that is shown in fig. 8. Figure 9 shows the effective $|\mathbf{k}|^2$ plot for both the $n\Sigma^-$ (${}^1S_0$) and $n\Sigma^-$ (${}^3S_1$) channels. The results of fitting the clear plateaus that are observed in both channels are shown in Table IV, and fig. 10 shows the results presented in Table IV normalized to the pion mass. The $n\Sigma^-$ (${}^1S_0$) channel is observed to have an interaction of natural size, and the energy that is measured in the calculation

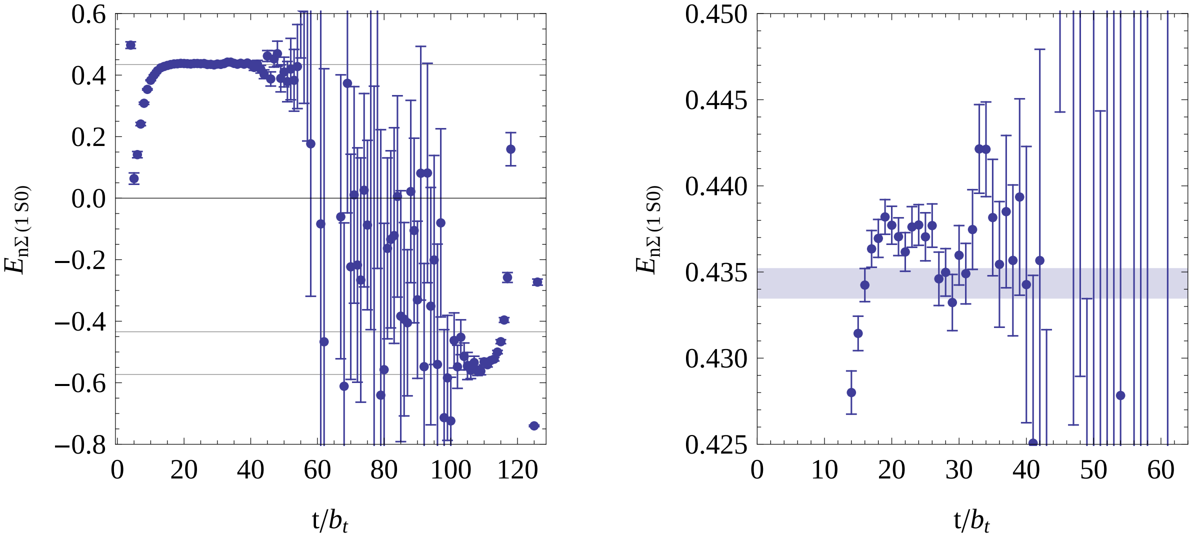

FIG. 7: The left panel is the $n\Sigma^-$ (${}^1S_0$) GEMP with $t_J = 1$, while the right panel shows the plateau region of the left panel. The band in the right panel and the upper line in the left panel correspond to $M_\Sigma + M_N$, while the lower two lines in the left panel correspond to $-(M_\Sigma + M_N)$ and $-(M_\Sigma + M_N + 2m_\pi)$, respectively.

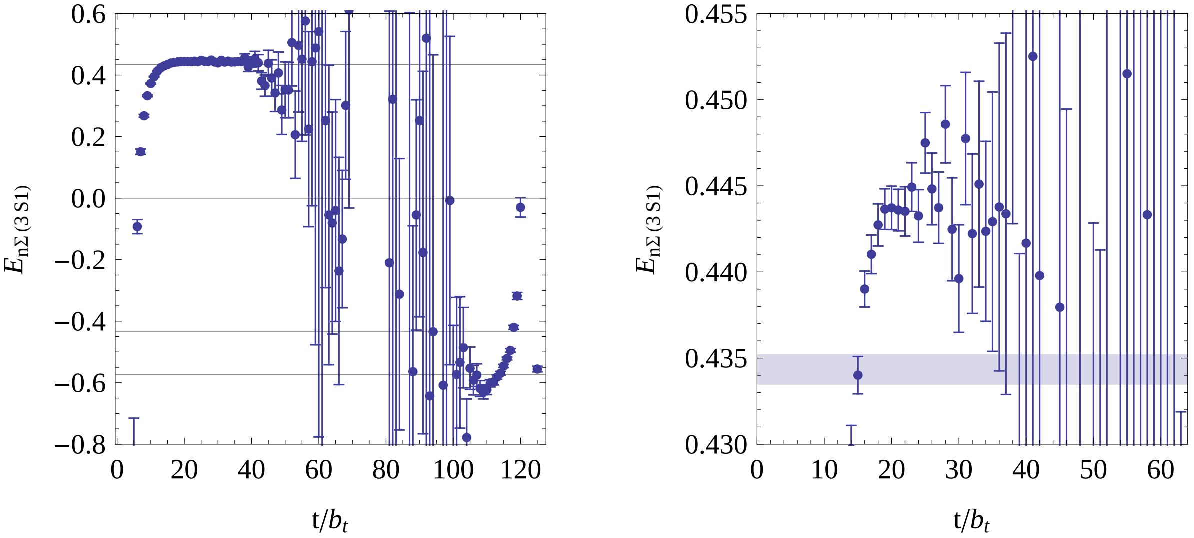

FIG. 8: The left panel is the $n\Sigma^-$ $(^3S_1)$ GEMP with $t_J = 1$, while the right panel shows the plateau region of the left panel. The band in the right panel and the upper line in the left panel correspond to $M_\Sigma + M_N$, while the lower two lines in the left panel correspond to $-(M_\Sigma + M_N)$ and $-(M_\Sigma + M_N + 2m_\pi)$, respectively.

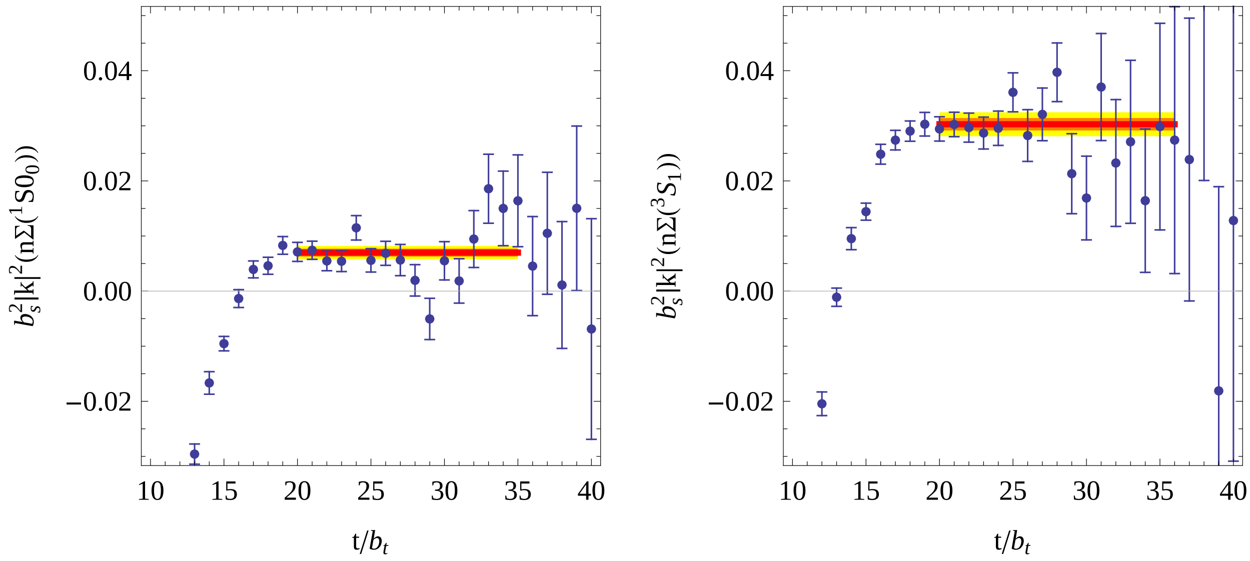

FIG. 9: The left panel is the effective $|\mathbf{k}|^2$ plot for the $n\Sigma^-$ $(^1S_0)$ channel with $t_J = 1$ and the fit to the plateau. The right panel is for the $n\Sigma^-$ $(^3S_1)$ channel.

lies within the regime of applicability of the effective-range expansion. In contrast, the interaction in the $n\Sigma^-$ $(^3S_1)$ channel is seen to be large, $|m_\pi/p\cot\delta(p)| \sim 3$, and is well

TABLE IV: Results for the strangeness $s = -1$ hyperon-nucleon channels.

Process	$\lvert\mathbf{k}\rvert^2/m_\pi^2$	ΔE (MeV)	$-1/p\cot\delta$ (fm)	χ^2/dof	fitting interval
$n\Sigma^-$ $(^1S_0)$	0.122(12)(19)	15.3(1.5)(2.3)	$0.361^{+0.025+0.038}_{-0.026-0.040}$	2.06	20 → 35
$n\Sigma^-$ $(^3S_1)$	0.551(17)(19)	67.9(2.1)(2.3)	$1.47^{+0.11+0.12}_{-0.09-0.11}$	0.91	19 → 36
$n\Lambda$ $(^1S_0)$	0.093(12)(19)	11.8(1.6)(2.3)	$0.297^{+0.036+0.051}_{-0.046-0.075}$	1.69	20 → 35
$n\Lambda$ $(^3S_1)$	0.094(15)(15)	11.9(1.9)(1.9)	$0.299^{+0.033+0.033}_{-0.036-0.036}$	1.05	20 → 35

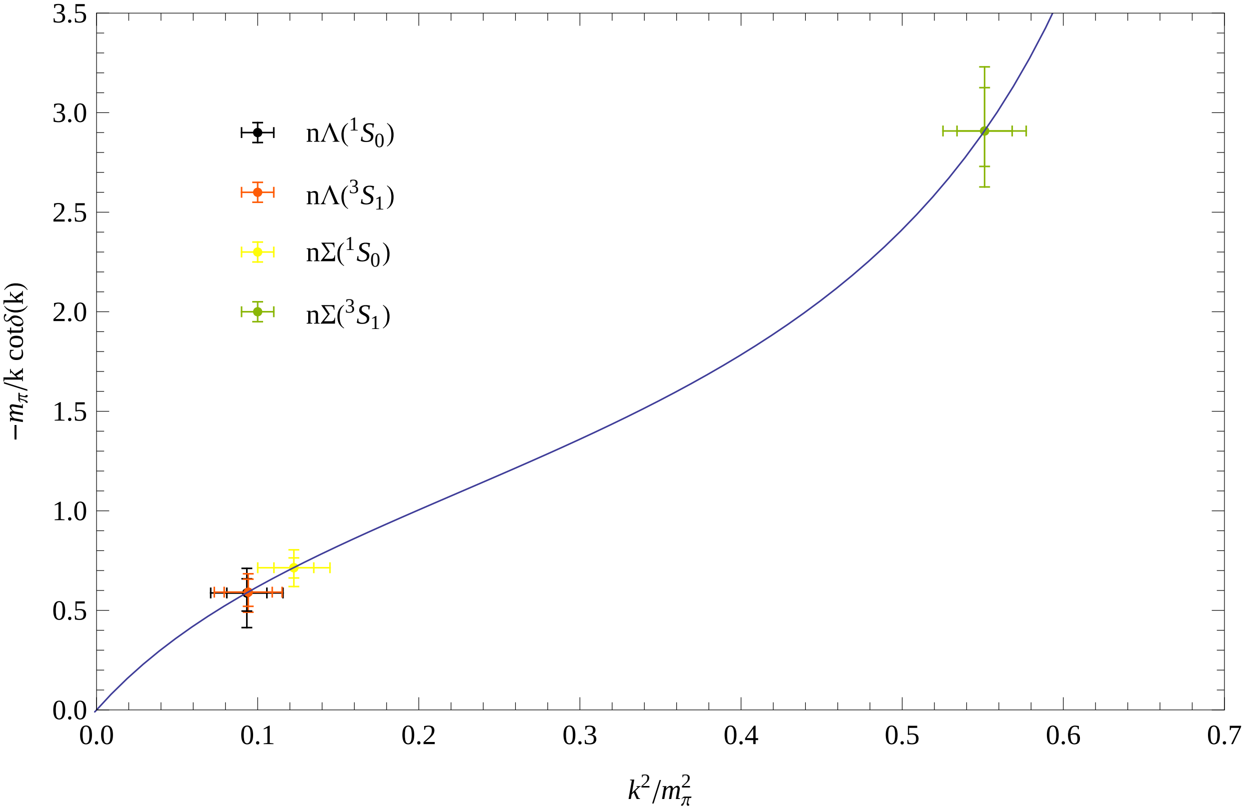

FIG. 10: The inverse of the real part of the inverse scattering amplitude normalized to the pion mass as a function of the squared-momentum in the center-of-mass of the baryons normalized to the pion mass. The dotted curve corresponds to the inverse "S-function", defined in eq. (8), from which $(k\cot\delta)^{-1}$ is determined from $\lvert\mathbf{k}\rvert^2$. The inner uncertainty of each data point is statistical and the outer uncertainty is the statistical and systematic uncertainty combined in quadrature.

outside the regime of applicability of the effective range expansion. At this momenta, the $n\Sigma^-$ $(^3S_1)$ is strongly interacting in a way that is consistent with an attractive interaction that supports a bound-state (which we find no direct evidence for in this calculation), or a repulsive interaction of unnaturally large range. These two scenarios cannot be resolved with calculations in a single volume, but ongoing calculations in different volumes will resolve this ambiguity. This result is perhaps the most important result of this present work. One concludes from this calculation that the $n\Sigma^-$ interaction is strongly spin-dependent.

2. *The coupled* $N\Lambda$*-* $N\Sigma$ *channel* ($I = \frac{1}{2}$)

The strangeness $s = -1$, isospin-$\frac{1}{2}$ energy-eigenstates in the lattice volume will, in general, couple to both the $N\Lambda$ and $N\Sigma$ channels. Therefore, the calculated $N\Lambda$ correlation functions will receive contributions from all such eigenstates in the volume. However, as $M_\Sigma - M_\Lambda = 0.0051$ t.l.u. is a significant mass splitting, we expect that a single-channel analysis is applicable in this system and proceed accordingly. Nevertheless, calculation of the isospin-$\frac{1}{2}$ $N\Sigma$ correlation function and the crossed correlation function resulting from a $N\Lambda$ source and a $N\Sigma$ sink would likely improve this analysis.

The GEMPs for the $n\Lambda$ ($^1S_0$) and $n\Lambda$ ($^3S_1$) correlation functions are shown in fig. 11 and 12, respectively, and in both cases a clear plateau is visible. Figure 13 shows the effective $|\mathbf{k}|^2$ plot for both the $n\Lambda$ ($^1S_0$) and $n\Lambda$ ($^3S_1$) channels and clear plateaus are again observed in both channels. The results of fitting to the plateau region of the effective $|\mathbf{k}|^2$ plots are reported in Table IV, and are displayed in fig. 10. The energy-splittings are both found to be $\Delta E \sim 0.002$ t.l.u, and are therefore smaller than the expected splitting between the energy eigenstates resulting from the $N\Lambda$-$N\Sigma$ mixing ($M_\Sigma - M_\Lambda = 0.0051$ t.l.u.). It therefore seems likely that, *a posteriori*, the single-channel analysis used here is applicable. The extracted squared-momenta and hence scattering amplitudes in the two spin channels

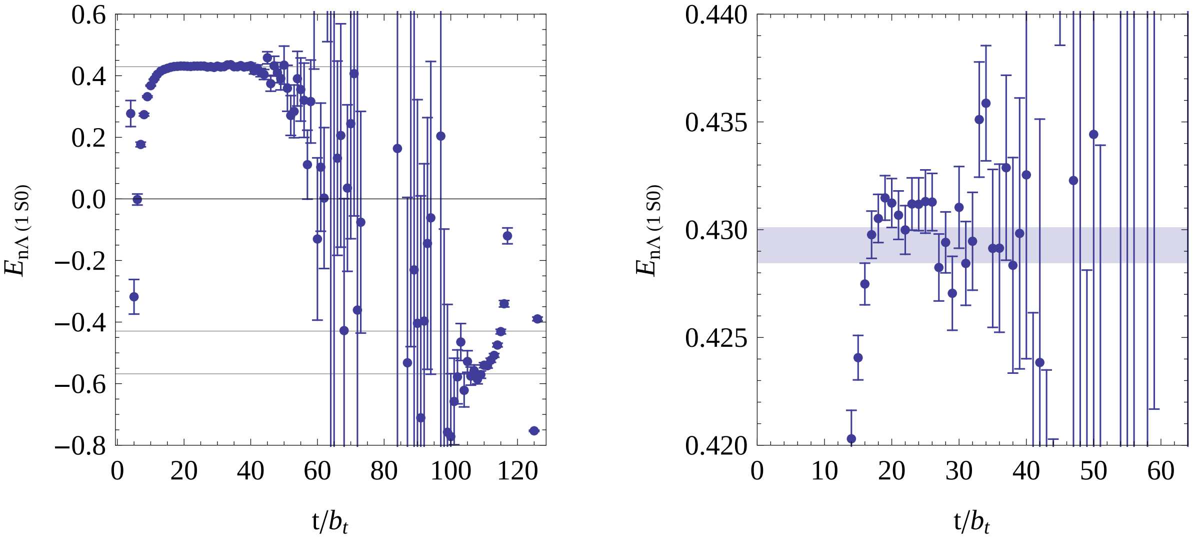

FIG. 11: The left panel is the $n\Lambda$ ($^1S_0$) GEMP with $t_J = 1$, while the right panel shows the plateau region of the left panel. The band in the right panel and the upper line in the left panel correspond to $M_\Lambda + M_N$, while the lower two lines in the left panel correspond to $-(M_\Lambda + M_N)$ and $-(M_\Lambda + M_N + 2m_\pi)$, respectively.

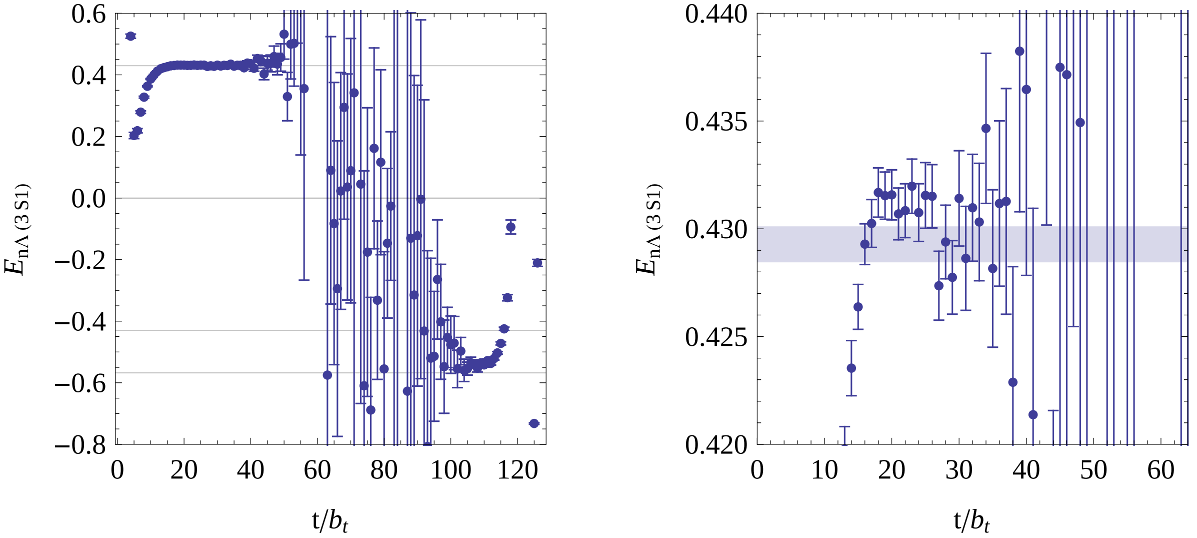

FIG. 12: The left panel is the $n\Lambda$ ($^3S_1$) GEMP with $t_J = 1$, while the right panel shows the plateau region of the left panel. The band in the right panel and the upper line in the left panel correspond to $M_\Lambda + M_N$, while the lower two lines in the left panel correspond to $-(M_\Lambda + M_N)$ and $-(M_\Lambda + M_N + 2m_\pi)$, respectively.

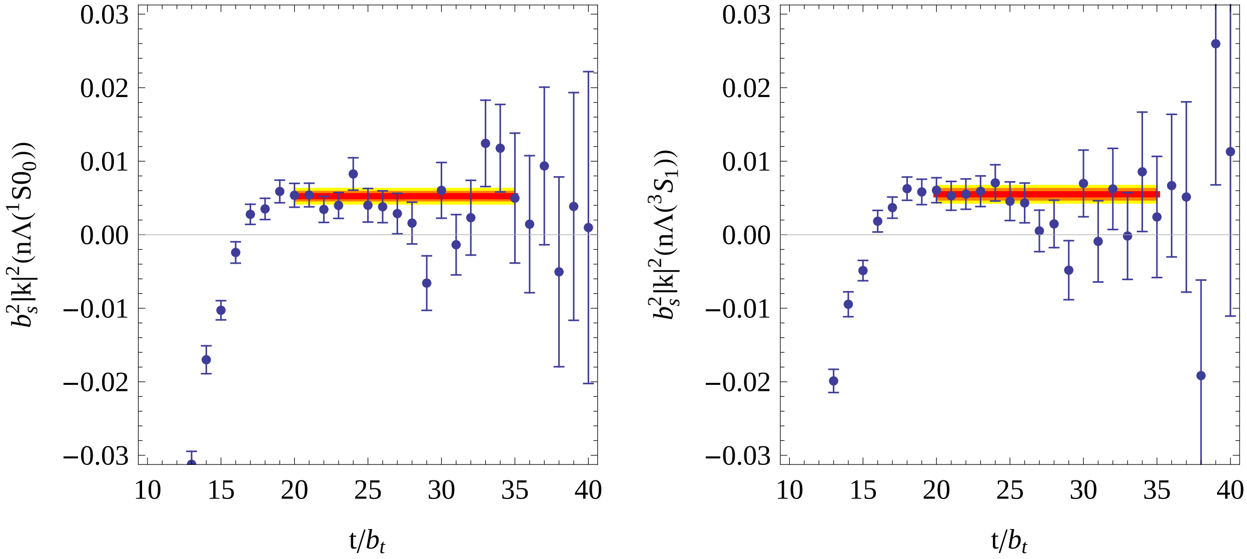

FIG. 13: The left panel is the effective $|\mathbf{k}|^2$ plot for the $n\Lambda$ ($^1S_0$) channel with $t_J = 1$ and the fit to the plateau. The right panel is for the $n\Lambda$ ($^3S_1$) channel.

are the same within uncertainties. This indicates that the spin-dependent interactions in these channels are very small. If the extracted states are predominately $N\Lambda$, then this result

TABLE V: A compilation of results for strangeness = −1 hyperon-nucleon scattering from lattice QCD. The columns labeled as "Valence" and "Sea" list the action used for the valence and sea quarks. A dash indicates a quenched calculation.

Process	m_π (MeV)	$\lvert\mathbf{k}\rvert$ (MeV)	$-1/p\cot\delta$ (fm)	Valence	Sea	Reference
$n\Lambda\ ^1S_0$	296(3)	50(26) i	−0.11(7)	Clover	Clover	[33]
$n\Lambda\ ^1S_0$	354(6)	255(26)	1.04(28)	DW	Staggered	[20]
$n\Lambda\ ^1S_0$	390.4(4.4)	119(14)	0.297(76)	Clover	Clover	present work
$n\Lambda\ ^1S_0$	465(1)	22(3) i	−0.09(3)	Clover	–	[33]
$n\Lambda\ ^1S_0$	493(8)	197(24)	0.63(12)	DW	Staggered	[20]
$n\Lambda\ ^1S_0$	514(1)	17(3) i	−0.07(3)	Clover	–	[33]
$n\Lambda\ ^3S_1$	296(3)	40(24) i	−0.07(7)	Clover	Clover	[33]
$n\Lambda\ ^3S_1$	354(6)	168(65)	0.50(27)	DW	Staggered	[20]
$n\Lambda\ ^3S_1$	390.4(4.4)	119(14)	0.299(49)	Clover	Clover	present work
$n\Lambda\ ^3S_1$	465(1)	24(3) i	−0.11(3)	Clover	–	[33]
$n\Lambda\ ^3S_1$	514(1)	20(2) i	−0.09(2)	Clover	–	[33]
$n\Sigma^-\ ^1S_0$	390.4(4.4)	136(12)	0.361(46)	Clover	Clover	present work
$n\Sigma^-\ ^1S_0$	493(8)	179(30)	0.57(14)	DW	Staggered	[20]
$n\Sigma^-\ ^3S_1$	390.4(4.4)	289.8(6.8)	1.47(16)	Clover	Clover	present work
$n\Sigma^-\ ^3S_1$	493(8)	261(37)	1.19(53)	DW	Staggered	[20]
$n\Sigma^-\ ^3S_1$	592(10)	226(30)	0.85(22)	DW	Staggered	[20]

is expected because of the fact that the long-range spin-dependent interaction resulting from OPE is absent (as the Λ is an isosinglet). Further, the extracted squared-momenta are consistent with that found in the $n\Sigma^-$ ($^1S_0$) channel.

3. Compilation of measurements

After the pioneering quenched calculations of YN scattering by Fukugita *et al* [28], and the first fully-dynamical $n_f = 2 + 1$ calculations [20], more refined quenched calculations have been performed along with one $n_f = 2+1$ calculation [33]. All of the results for $s = -1$ YN scattering that have been obtained from lattice QCD calculations are shown in Table V. As the measurements have been performed at different pion masses and in different lattice volumes, resulting in different center-of-mass energies, it is difficult to present these results in a single diagram. The present measurements and the mixed-action measurements [20] were both on lattices with spatial volumes of $V \sim (2.5\text{ fm})^3$, and with a lattice spacing of $b \sim 0.125$ fm and so a direct comparison is possible for this subset of measurements.

C. Hyperon-hyperon interactions ($s = -2$)

Lattice QCD calculations of hyperon-hyperon interactions are important as they can provide guidance to the experimental programs in hyper-nuclear physics. They can also improve upon the current understanding of the stability of the core of supernovae if it becomes energetically favorable to have strange baryons present. To this end we have calculated the correlation functions resulting from $\Lambda\Lambda$ and $\Sigma^-\Sigma^-$ sources and sinks. The $\Sigma^-\Sigma^-$ channel has $I_z = -2$ and, as such, a single, isolated ground-state is expected which can be used to determine the $\Sigma^-\Sigma^-$ scattering phase shift with a single-channel analysis. In contrast, the correlation function produced by the $\Lambda\Lambda$ source is expected to exhibit two nearly degenerate states as $2M_\Lambda = 0.44492$ t.l.u. and $M_\Xi + M_N = 0.44783$ t.l.u.. Further, the $\Sigma^+\Sigma^-$ state is likely to be close by, $2M_\Sigma = 0.45504$ t.l.u.. An operator of the form $\Xi^- p$ would help to resolve the states, but we have not calculated this correlation function, nor the possible mixed correlation functions. Further, we have not explored the isospin-1 channels, such as the $N\Xi - \Lambda\Sigma$ coupled channels, but we would expect to find very-closely spaced energy eigenstates for the pion mass used in this calculation, making clean extractions very difficult. In particular, $M_{\Xi^-} + M_n = 0.449$ t.l.u while $M_\Lambda + M_{\Sigma^-} = 0.452$ t.l.u. Quenched calculations of the $p\Xi^0$ scattering length have been presented in Ref. [34].

1. $\Lambda\Lambda$ *interactions* $(I = 0)$

The low-lying eigenstates that couple to a $\Lambda\Lambda$ source and sink are, in principle, linear combinations of all two-baryon states with $s = -2$ and $I = 0$, namely, $\Lambda\Lambda$, $\Sigma\Sigma$, $N\Xi$ and their excitations. The GEMP for the $\Lambda\Lambda$ channel (for a particular combination of SP and SS correlation functions) is shown in fig. 14, in which a clear plateau is observed. The effective $|\mathbf{k}|^2$ plot shown in fig. 15 also shows a clear plateau that is negative shifted in energy, unambiguously indicating an attractive interaction. The energy of this state is the lowest,

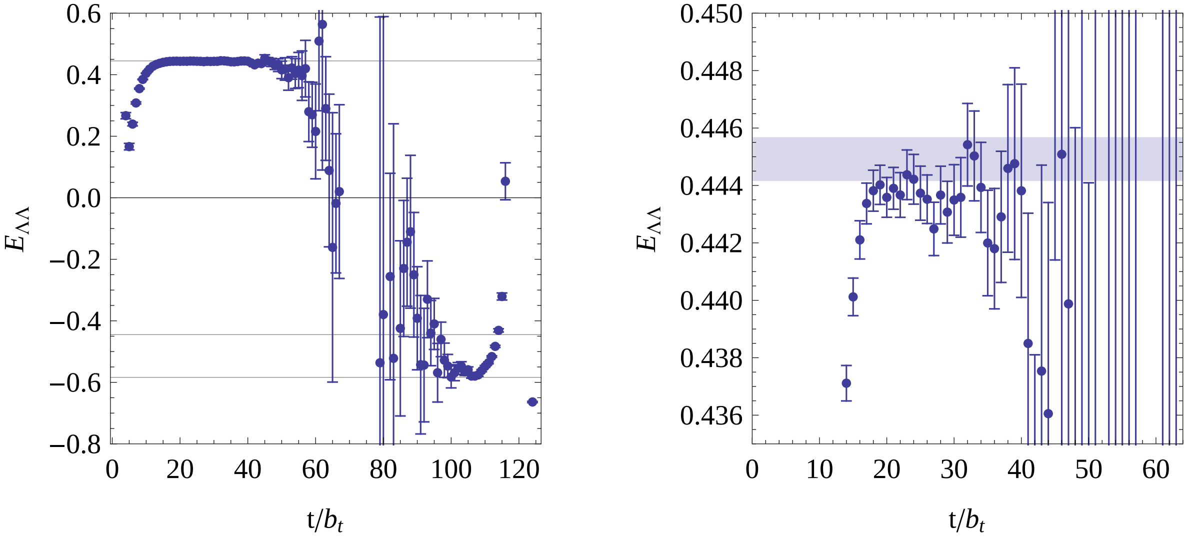

FIG. 14: The left panel is the $\Lambda\Lambda$ GEMP with $t_J = 3$, while the right panel shows the plateau region of the left panel. The band in the right panel and the upper line in the left panel correspond to $2M_\Lambda$, while the lower two lines in the left panel correspond to $-2M_\Lambda$ and $-2(M_\Lambda + m_\pi)$, respectively.

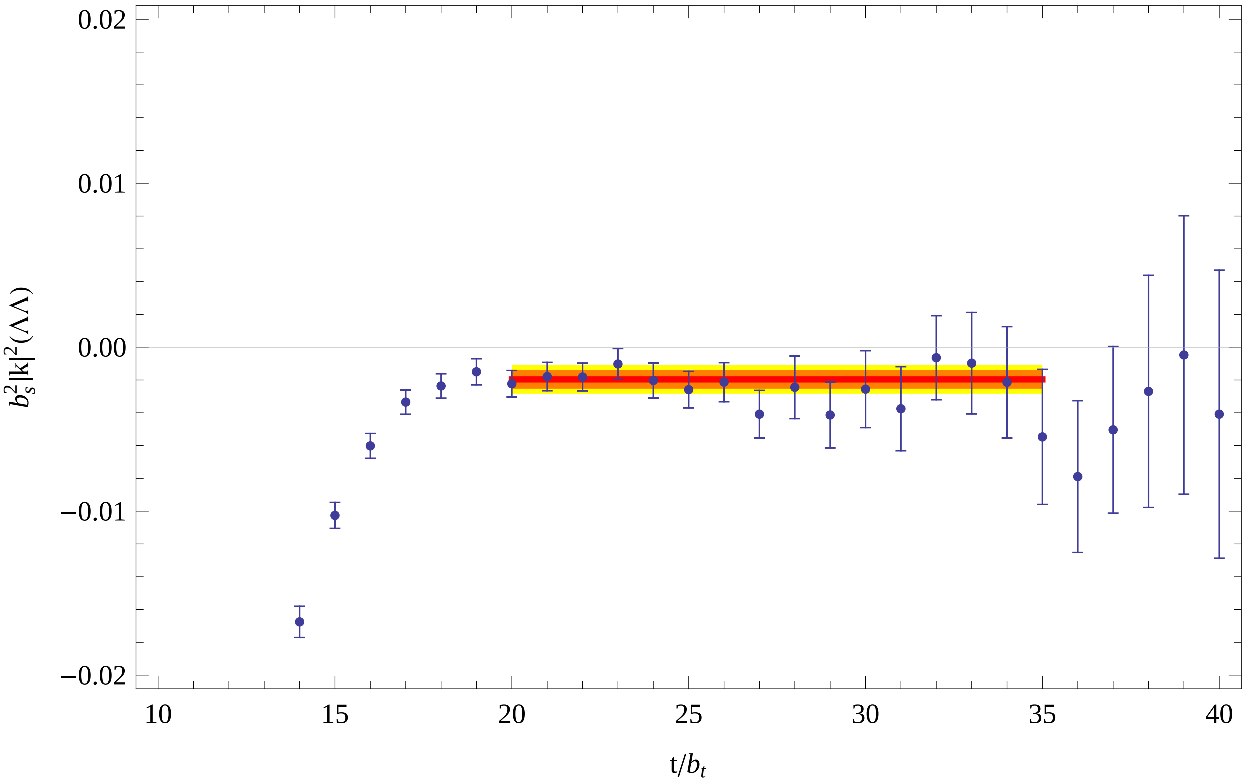

FIG. 15: The effective $|\mathbf{k}|^2$ plot for the $\Lambda\Lambda$ channel with $t_J = 3$ and the fit to the plateau.

and the plateau is the longest, for any combination of SS and SP correlation functions that could be constructed. Other combinations of correlation functions suggest states at higher energies, consistent with expectations of nearby states, however, with the current data, no definitive statements can be made. The splittings between the asymptotic states, $\Lambda\Lambda$ and $N\Xi$ are such that at measured (very small) $\Lambda\Lambda$ center-of-mass momentum a single-channel analysis can be performed to define the $\Lambda\Lambda$ elastic scattering amplitude, the results of which are shown in Table VI, and shown graphically in fig. 16.

TABLE VI: Results for the strangeness = −2 and strangeness = −4 hyperon-hyperon channels.

Process	$\lvert\mathbf{k}\rvert^2/m_\pi^2$	ΔE (MeV)	$-1/p\cot\delta$ (fm)	χ^2/dof	fitting interval
$\Lambda\Lambda$	−0.033(09)(11)	−4.1(1.2)(1.4)	$-0.188^{+0.062+0.072}_{-0.072-0.085}$	1.38	20 → 35
$\Sigma^-\Sigma^-$	0.215(11)(18)	25.5(1.3)(2.1)	$0.534^{+0.019+0.032}_{-0.019-0.032}$	2.6	20 → 36
$\Xi^-\Xi^-$	0.0247(94)(77)	2.8(1.1)(0.9)	$0.101^{+0.032+0.026}_{-0.036-0.029}$	1.56	21 → 34

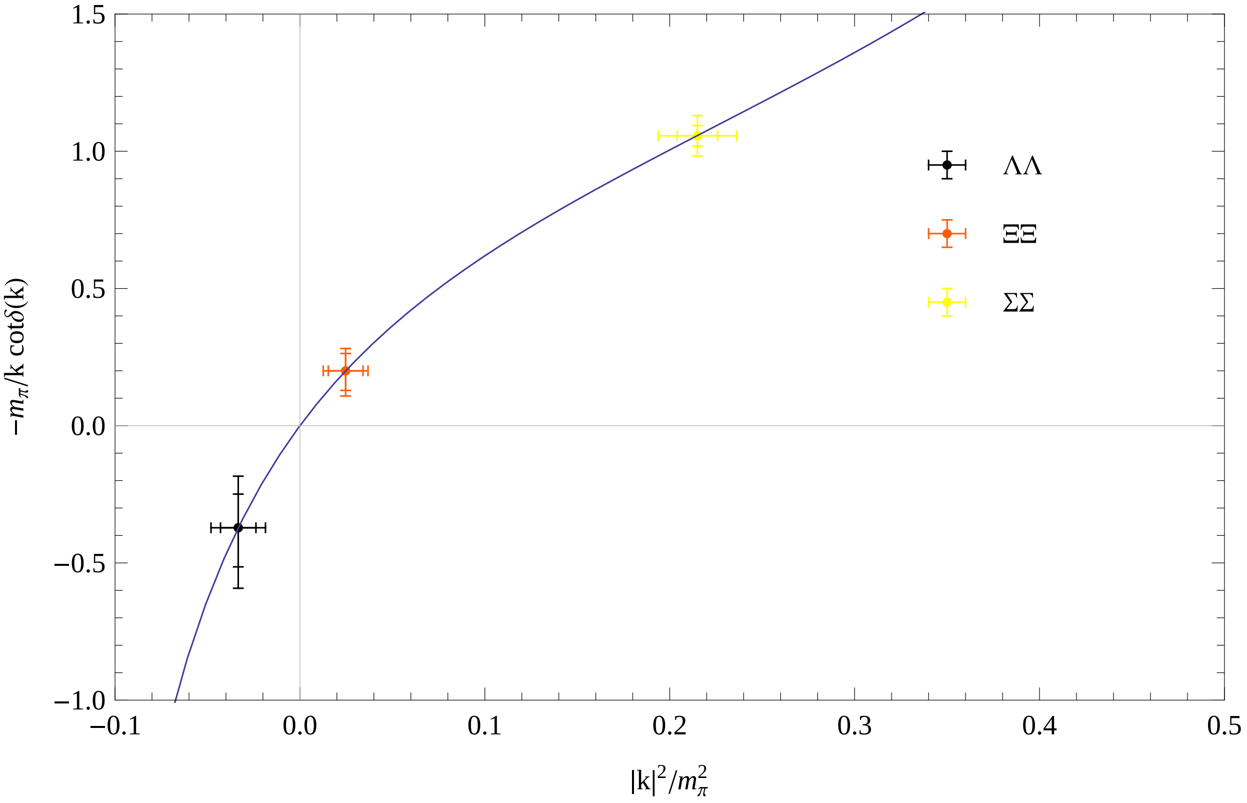

FIG. 16: The inverse of the real part of the inverse scattering amplitude normalized to the pion mass as a function of the squared-momentum in the center-of-mass of the baryons normalized to the pion mass. The dotted curve corresponds to the inverse "S-function", defined in eq. (8), from which $(k \cot \delta)^{-1}$ is determined from $|\mathbf{k}|^2$. The inner uncertainty of each data point is statistical and the outer uncertainty is the statistical and systematic uncertainty combined in quadrature.

The $\Lambda\Lambda$ channel is the only channel in which a negatively-shifted energy splitting is observed. However, without performing measurements on additional lattice volumes, it is presently not possible to determine if this negative energy shift indicates the presence of a bound state (the infamous H-dibaryon [35]) or if it is simply a continuum state that is negatively shifted due to an attractive interaction. The location of the state on the "S-function" curve suggests that it is fact a continuum state [8], but further measurements are required to properly explore this exciting possibility.

2. $\Sigma^-\Sigma^-$ interactions ($I = 2$)

Due to its quantum numbers, $s = -2$ and $I = 2$, the $\Sigma^-\Sigma^-$ channel is not expected to have other states near the ground state in the lattice volume as there are no other states comprised of two octet baryons with these quantum numbers. The GEMP associated with the $\Sigma^-\Sigma^-$ correlation function is shown in fig. 17 and the resulting effective $|\mathbf{k}|^2$ plot is shown in fig. 18. The results obtained by fitting to the effective $|\mathbf{k}|^2$ plot are shown in Table VI above, and presented graphically in fig. 16. The somewhat large value of $\chi^2/\text{dof} = 2.6$ is due to the downward fluctuation near time-slice $t = 29$ in fig. 18, which we assume to be statistical in nature. A smaller fitting interval would yield approximately the same scattering

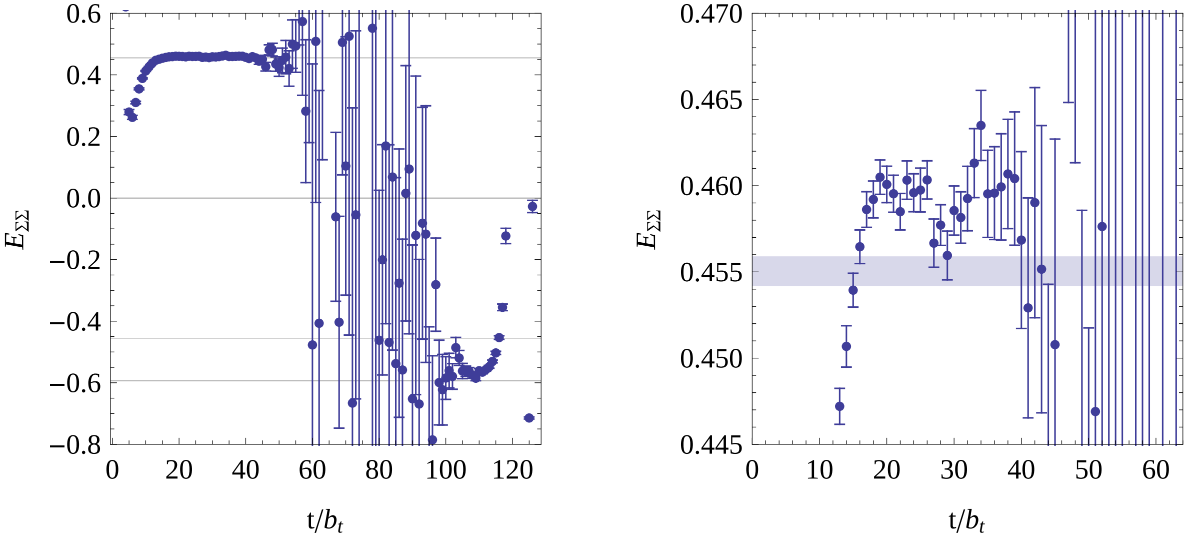

FIG. 17: The left panel is the $\Sigma^-\Sigma^-$ GEMP with $t_J = 1$, while the right panel shows the plateau region of the left panel. The band in the right panel and the upper line in the left panel correspond to $2M_\Sigma$, while the lower two lines in the left panel correspond to $-2M_\Sigma$ and $-2(M_\Sigma + m_\pi)$, respectively.

phase shift, but with a substantially smaller χ^2/dof.

D. Hyperon-hyperon interactions ($s = -4$)

Baryon-baryon interactions in the strangeness -4 sector have no obvious phenomenological implications. However, it is found that systems containing heavier quarks, such as the Ω or Ξ, have better-behaved correlation functions in lattice QCD calculations. As lattice QCD calculations of hadronic interactions are still in their infancy, it is useful to explore such systems to better understand aspects of the methodology that we employ.

The only $s = -4$ systems of two octet-baryons are the $I = 0, 1$ $\Xi\Xi$ combinations and here we focus on $I = 1$ ($\Xi^-\Xi^-$). The low-lying states in the lattice volume that couple to the $\Xi^-\Xi^-$ interpolating operator are expected to be describable in terms of a single-channel elastic-scattering amplitude as there are no other states composed of two octet baryons that can couple to them. The GEMPs for this channel are shown in fig. 19, and the resulting effective $|\mathbf{k}|^2$ plot is shown in fig. 20. The results obtained by fitting to the effective $|\mathbf{k}|^2$ plot are shown in Table VI, and presented graphically in fig. 16, normalized to the pion mass. The effective $|\mathbf{k}|^2$ plot shows the downward fluctuation seen in other correlators at time-slice $t = 29$, and the resulting fit is consistent with zero at the 2σ-level. We conclude that the $\Xi^-\Xi^-$ interactions at this value of the pion mass are quite weak.

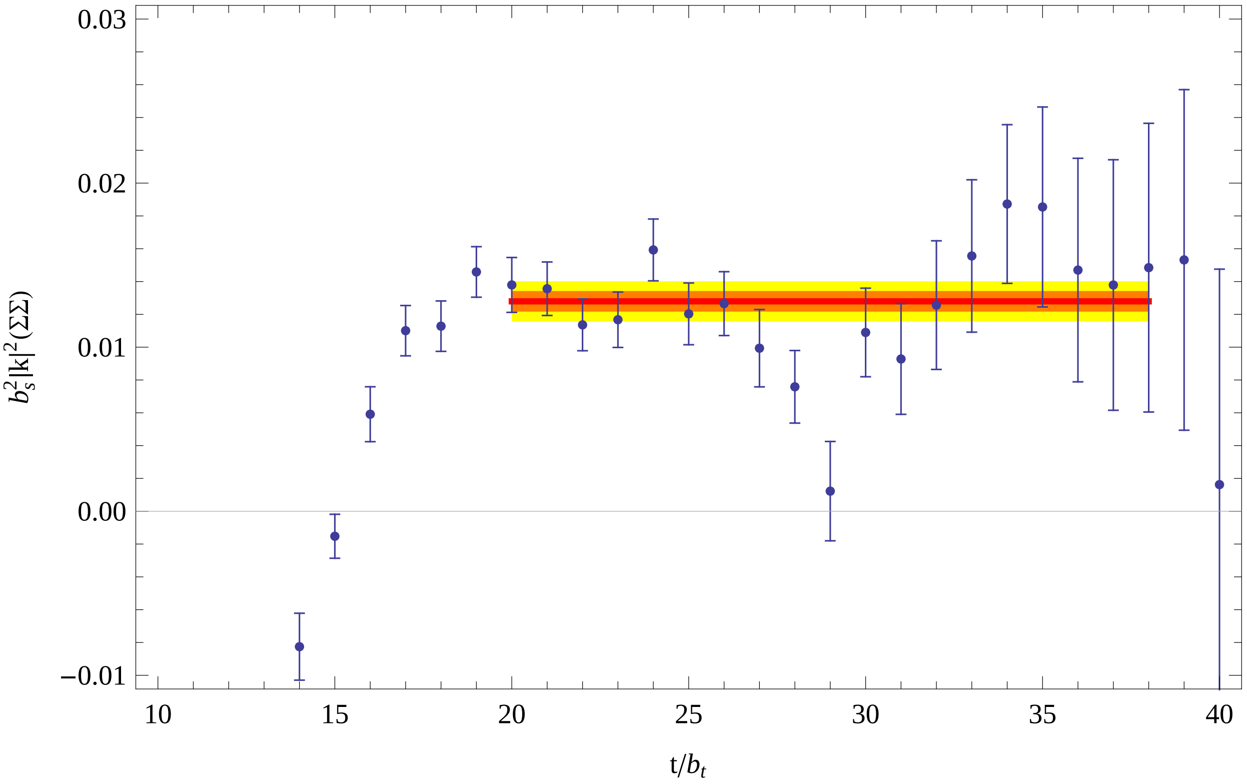

FIG. 18: The effective $|\mathbf{k}|^2$ plot for the $\Sigma^-\Sigma^-$ channel with $t_J = 1$ and the fit to the plateau.

V. STATISTICAL SCALING AND NOISE IN CORRELATION FUNCTIONS

The precision of lattice QCD calculations of any quantity is limited by the statistical noise in the relevant correlation functions. Until recently [22, 23], the lore has been (based on general arguments by Lepage [18]) that the signal-to-noise ratios in (multi-)baryon correlation functions degrade exponentially with time and with the number of baryons in the system. In Refs. [22, 23], we showed that, while this behavior is observed at large times, at intermediate times the signal-to-noise ratio does not degrade exponentially, and in fact it is found to be independent of time for a significant number of time slices (the "Golden Window") for the sources that are used. Further, in this window of time-slices, the signal-to-noise ratio is essentially independent of the number of baryons in the system.

After reviewing Lepage's arguments regarding the general behavior of signal-to-noise ratio, and their generalization to the temporal boundary conditions that are used in the present work, a thorough exploration of the noise in the various correlators of the two-baryon sector is presented.

A. Aspects of the noise correlation functions and the signal-to-noise ratio

On gauge-field configurations with infinite temporal extent, correlation functions of one or more baryons exhibit statistical noise at large-times that increases exponentially with Euclidean time [18]. In the case of a source that has the quantum numbers of a single

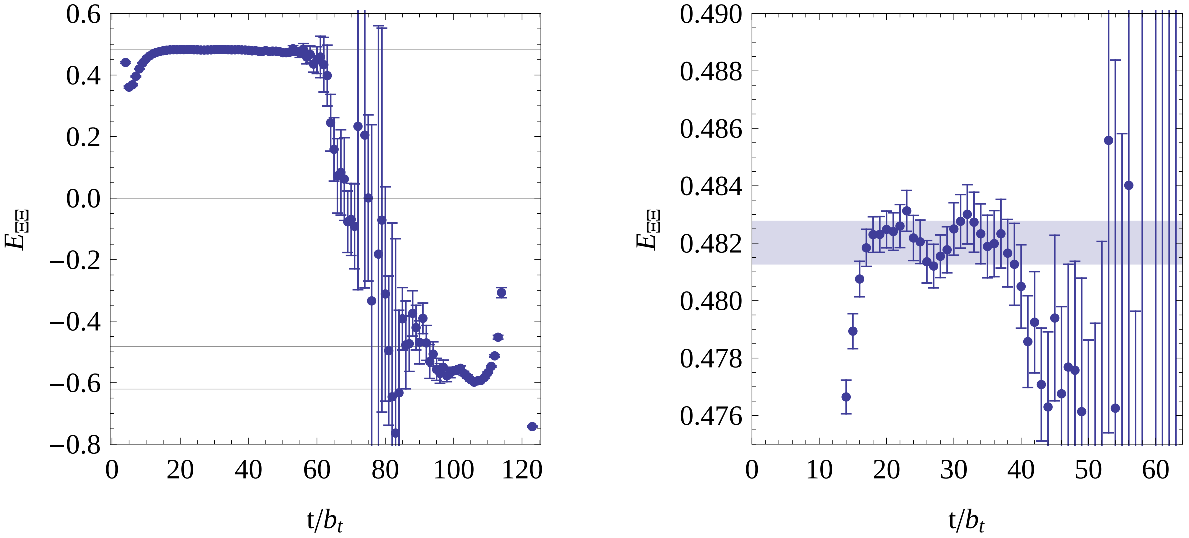

FIG. 19: The left panel is the $\Xi^-\Xi^-$ GEMP with $t_J = 1$, while the right panel shows the plateau region of the left panel. The band in the right panel and the upper line in the left panel correspond to $2M_\Xi$, while the lower two lines in the left panel correspond to $-2M_\Xi$ and $-2(M_\Xi + m_\pi)$, respectively.

positive parity nucleon, the correlation function has the form

$$\langle \theta_N(t) \rangle \ = \ \sum_{\mathbf{x}} \ \Gamma_+^{\beta\alpha} \ \langle 0| \ N^\alpha(\mathbf{x},t) \overline{N}^\beta(\mathbf{0},0) \ |0\rangle \ \rightarrow \ Z_N \ e^{-M_N t} \quad , \tag{13}$$

where $N^\alpha(\mathbf{x},t)$ is an interpolating field (composed of three quark operators) that has non-vanishing overlap with the nucleon, Γ_+ is a positive energy projector, and the angle brackets indicate statistical averaging over measurements on an ensemble of configurations. The variance of this correlation function is given by

$$\begin{aligned} \mathrm{N}\ \sigma^2 \ &\sim \ \langle \theta_N^\dagger(t) \theta_N(t) \rangle - \langle \theta_N(t) \rangle^2 \\ &= \ \sum_{\mathbf{x},\mathbf{y}} \Gamma_+^{\delta\alpha} \Gamma_+^{\gamma\beta\dagger} \ \langle 0| \ N^\alpha(\mathbf{x},t) \overline{N}^\beta(\mathbf{y},t) N^\gamma(\mathbf{0},0) \overline{N}^\delta(\mathbf{0},0) \ |0\rangle \ \ - \ \langle \theta_N(t) \rangle^2 \\ &\rightarrow \ Z_{N\overline{N}} e^{-2M_N t} - Z_N^2 e^{-2M_N t} \ + \ Z_{3\pi} \ e^{-3m_\pi t} \ + \ \ldots \ \overset{t\rightarrow\infty}{\rightarrow} \ Z_{3\pi} \ e^{-3m_\pi t} \quad , \end{aligned} \tag{14}$$

where all interaction energies have been neglected, and N is the number of (independent) measurements (distinct from the nucleon field operator N). At large times, the noise-to-signal ratio consequently behaves as [18]

$$\frac{\sigma}{\overline{x}} \ = \ \frac{\sigma(t)}{\langle \theta(t) \rangle} \sim \frac{1}{\sqrt{\mathrm{N}}} \ e^{\left(M_N - \frac{3}{2} m_\pi\right) t} \quad . \tag{15}$$

More generally, for a system of A nucleons, the noise-to-signal ratio behaves as

$$\frac{\sigma}{\overline{x}} \ \ \sim \frac{1}{\sqrt{\mathrm{N}}} \ e^{A\left(M_N - \frac{3}{2} m_\pi\right) t} \tag{16}$$

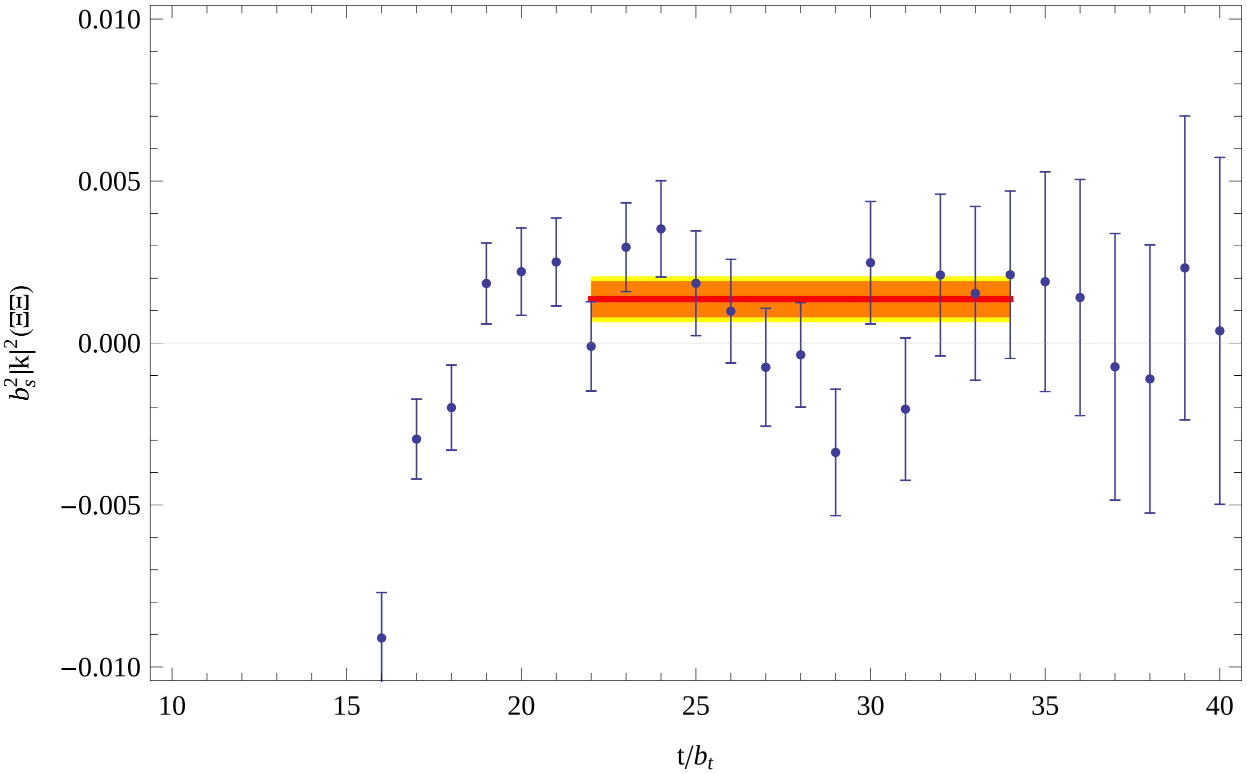

FIG. 20: The effective $|\mathbf{k}|^2$ plot for the $\Xi^-\Xi^-$ channel with $t_J = 3$ and the fit to the plateau.

at large times.

As we discussed in Ref. [23], the various "Z-factors", such as $Z_{3\pi}$, depend upon the details of the sources and sinks interpolators that are used. For the present calculations, the projection onto zero-momentum final state nucleons, introduces a $1/\sqrt{\text{Volume}}$ suppression of the amplitudes of the various components (except for $N\overline{N}$) in addition to color and spin rearrangement suppressions that exists independent of the spatial structure of the source. As a consequence, an interval of time slices exists at short times (the "Golden Window") in which the variance of the correlation function is dominated by the terms in eq. (14) that behave as $\sim e^{-2M_N t}$. In this window, the signal-to-noise ratio of the single baryon correlation function is independent of time. Further, the signal-to-noise ratio does not degrade exponentially faster in multi-baryon correlation functions than in single-baryon correlation functions in the "Golden Window" [23].

The finite temporal extent introduces backward propagating states (thermal states) into the correlation functions which lead to exponentially worse signal-to-noise ratios at large times [22, 23]. These contributions are suppressed by at least $\exp(m_\pi T)$, however, in the present work (where $m_\pi T \sim 9$), these effects cause complications. We note that the impact of these states can be mitigated by working at larger temporal extents and exponentially large computational resources are not required to remove this effect.

With the high statistics that have been accumulated in the present work, the behavior of the signal-to-noise ratio can be carefully examined. It is useful to form the effective noise-to-signal plot [22], in analogy with the GEMPs. On each time slice, the quantity

$$\mathcal{S}(t) \ = \ \frac{\sigma(t)}{\overline{x}(t)} \quad , \tag{17}$$

is formed, from which the energy governing the exponential behavior (the signal-to-noise energy-scale) can be extracted via

$$E_s(t;t_J) \;=\; \frac{1}{t_J}\,\log\left(\frac{\mathcal{S}(t+t_J)}{\mathcal{S}(t)}\right) \quad . \tag{18}$$

For a correlation function that is dominated by a single state with a corresponding variance correlation function dominated by a single energy scale, the quantity $E_s(t;t_J)$ will be independent of both t and t_J.

B. Measured signal-to-noise ratios in the one and two nucleon sectors

In the single nucleon sector, we expect that the energy scales $E_s \sim 0$, $M_N - \frac{3}{2}m_\pi$, and others, contribute to the signal-to-noise ratio. At times when the nucleon correlation function is in the ground state, and the variance correlation function is dominated by the nucleon-antinucleon state, $E_s = 0$ should dominate the signal-to-noise ratio. At large times the variance correlation function is dominated by the 3-pion state and $E_s = M_N - \frac{3}{2}m_\pi$ should dominate. This is modified by the finite temporal direction [22] as the hadrons produced by the sources of the correlation function and the variance correlation function can propagate forward and backward in time. The measured energy scale of the signal-to-noise ratio of the single nucleon correlation function is shown in fig. 21. It exhibits behavior that is consistent with expectations, and exceeds the long-time behavior expected from the Lepage argument at approximately time-slice $t = 50$ due to the temporal boundary conditions.

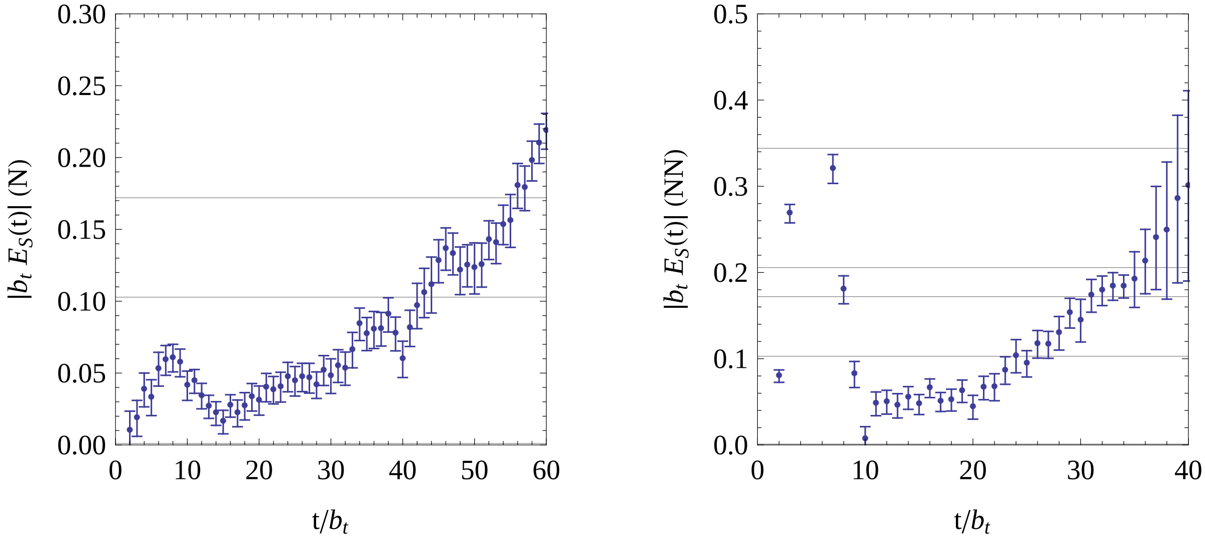

FIG. 21: The energy scale of the signal-to-noise ratio in the nucleon (left panel) and proton-proton (right panel) correlation functions, as defined in eq. (18), with $t_J = 6$. The horizontal lines in the left panel correspond to $E_s = 0$, $M_N - \frac{3}{2}m_\pi$ and $M_N - \frac{1}{2}m_\pi$, while those in the right panel correspond to $E_s = 0$, $M_N - \frac{3}{2}m_\pi$, $M_N - \frac{1}{2}m_\pi$, $2M_N - 3m_\pi$, $2M_N - m_\pi$.

On configurations with infinite temporal extent, the proton-proton correlation function is of the form (neglecting interactions between the hadrons)

$$\begin{aligned} \langle \theta_{NN}(t) \rangle \ &= \ \sum_{\mathbf{x},\mathbf{y}} \Gamma_{+}^{\alpha\gamma\beta\rho} \ \langle 0| \ N^\alpha(\mathbf{x},t) N^\gamma(\mathbf{y},t) \overline{N}^\beta(\mathbf{0},0) \overline{N}^\rho(\mathbf{0},0) \ |0\rangle \\ &\rightarrow \ Z_{NN} \ e^{-2M_N t} + \ldots , \end{aligned} \tag{19}$$

and the variance correlation function has the form

$$\begin{aligned} \mathrm{N} \ \sigma^2 \ &\sim \ \langle \theta_{NN}^\dagger(t) \theta_{NN}(t) \rangle - \langle \theta_{NN}(t) \rangle^2 \\ &= \ \sum_{\mathbf{x},\mathbf{y},\mathbf{z},\mathbf{w}} \Gamma_{+}^{\alpha\rho\delta\psi} \Gamma_{+}^{\beta\eta\gamma\zeta\dagger} \ \langle 0| \ N^\alpha(\mathbf{x},t) N^\rho(\mathbf{y},t) \overline{N}^\beta(\mathbf{z},t) \overline{N}^\eta(\mathbf{w},t) \ \times \\ &\qquad\qquad \overline{N}^\delta(\mathbf{0},0) \overline{N}^\psi(\mathbf{0},0) N^\gamma(\mathbf{0},0) N^\zeta(\mathbf{0},0) \ |0\rangle \ - \ \langle \theta_{NN}(t) \rangle^2 \\ &\rightarrow \ Z_{NN\overline{NN}} e^{-4M_N t} - Z_{NN}^2 e^{-4M_N t} \ + \ Z_{3\pi N\overline{N}} \ e^{-(2M_N + 3m_\pi)t} + Z_{6\pi} \ e^{-6m_\pi t} + \ldots \\ &\rightarrow \ Z_{6\pi} \ e^{-6m_\pi t} . \end{aligned} \tag{20}$$

Therefore, we anticipate finding energy scales of approximately $E_s = 0, M_N - \frac{3}{2}m_\pi$ and $2M_N - 3m_\pi$ in the signal-to-noise ratio on gauge-field configurations of infinite temporal extent. The temporal boundary conditions imposed in the present calculation introduce additional energy scales due to the backward propagating states.

Figure 22 shows the energy scale associated with the signal-to-noise ratio for the ratio of correlation functions that provides the energy splitting between two interacting protons and two isolated protons from which the $p \cot \delta(p)$ is extracted. It is clear that the energy scale of the energy splitting is significantly less than for the individual energies, and is consistent with zero throughout much of the Golden Window of time slices. This indicates that the signal-to-noise ratio associated with the energy splitting in the proton-proton sector, and hence the scattering parameters and bound-state energies, are time independent for the sources and sinks used here, and therefore do not degrade exponentially with time. This is an exceptionally important result, as it means that the extraction of NN, and more generally, multi-nucleon interactions, does not require an exponentially large number of measurements for each relevant correlation function. Further exploration and discussion of this point can be found in our work on three baryon systems [23].

C. Measured signal-to-noise ratios in the $N\Sigma$ sector

The discussion of the behavior of the signal-to-noise ratio in the YN sector parallels that in the multi-nucleon sector in section V B. An important difference is the presence of the strange quark, and the associated strange hadrons. The lowest energy scale contributing to the signal-to-noise ratio (beyond $E_s = 0$) is $E_s = M_N - \frac{3}{2}m_\pi$, and so it is expected that the degradation of the signal-to-noise ratio will be similar to that found in the NN correlations functions. It is found that the associated energy scale in the $n\Sigma^-$ $({}^3S_1)$ channel, as shown in fig. 23, is somewhat less than $M_N - \frac{3}{2}m_\pi$ over a number of time-slices, and starts to exceed this value for time-slices greater than $t \gtrsim 20$.

The energy scale associated with the signal-to-noise ratio in the difference in energy between $N\Sigma$ interacting in the ${}^3S_1$-channel and $M_N + M_\Sigma$ is shown in fig. 24. The energy scale seems to be somewhat larger than in the NN sector, and is non zero throughout the

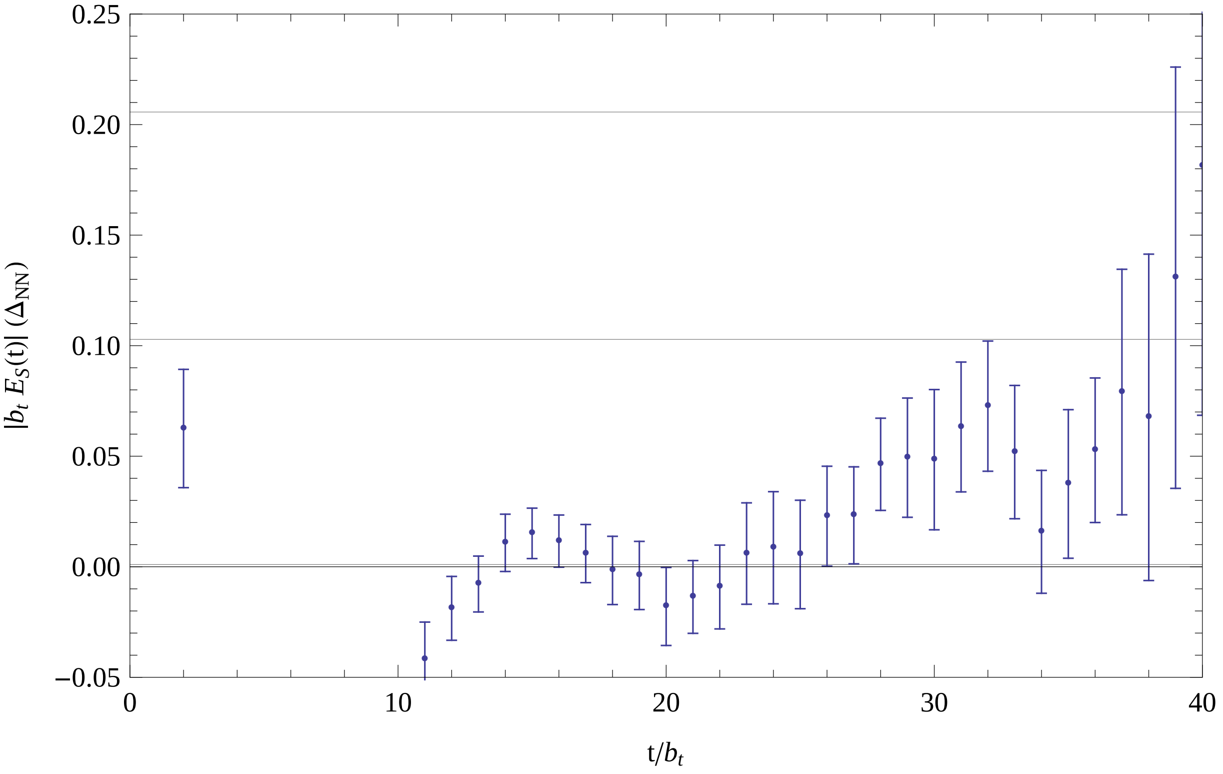

FIG. 22: The energy scale of the signal-to-noise ratio, as defined in eq. (18), in the ratio of correlation functions that produces the shift in energy between two interacting protons and two isolated protons, with $t_J = 6$. The horizontal lines correspond to $E_s = 0$, $M_N - \frac{3}{2}m_\pi$ and $2M_N - 3m_\pi$.

Golden Window. The interaction is strong in this channel, and therefore a non-zero value of E_s in the plateau region is not surprising.

D. Measured signal-to-noise ratios in the one and two Ξ sectors

The signal-to-noise ratio in the $\Xi\Xi$ sector is noticeably better than in the NN and the YN sectors. The energy scale associated with the Ξ and $\Xi^-\Xi^-$ correlation functions are shown in fig. 25. The lowest energy scale contributing to the signal-to-noise ratio in the single Ξ correlation function (beyond $E_s = 0$) is $E_s = M_\Xi - m_K - \frac{1}{2}m_\eta$. It is clear from the left panel in fig. 25 that the scale is much lower than this until time-slice $t \sim 50$. The situation is similar in the $\Xi^-\Xi^-$ correlation function in which the energy scale associated with the signal-to-noise ratio is found to be much less than the anticipated $E_s = M_\Xi - m_K - \frac{1}{2}m_\eta$ (beyond $E_s = 0$) until time-slice $t \sim 40$. Further, as shown in fig. 26, the energy scale associated with the energy splitting between the $\Xi^-\Xi^-$ state and two isolated Ξ^-'s is very small, and consistent with zero, for many time-slices below $t \lesssim 35$, and increases slowly beyond this.

It is likely that the improved signal-to-noise behavior in the $\Xi\Xi$ sector is due to a reduced overlap of the source onto the multi-meson intermediate states in the variance correlation function compared to purely baryonic intermediate states. Such a reduction is expected based on the fact that the volume occupied by multiple Ξ's is smaller than that of multiple

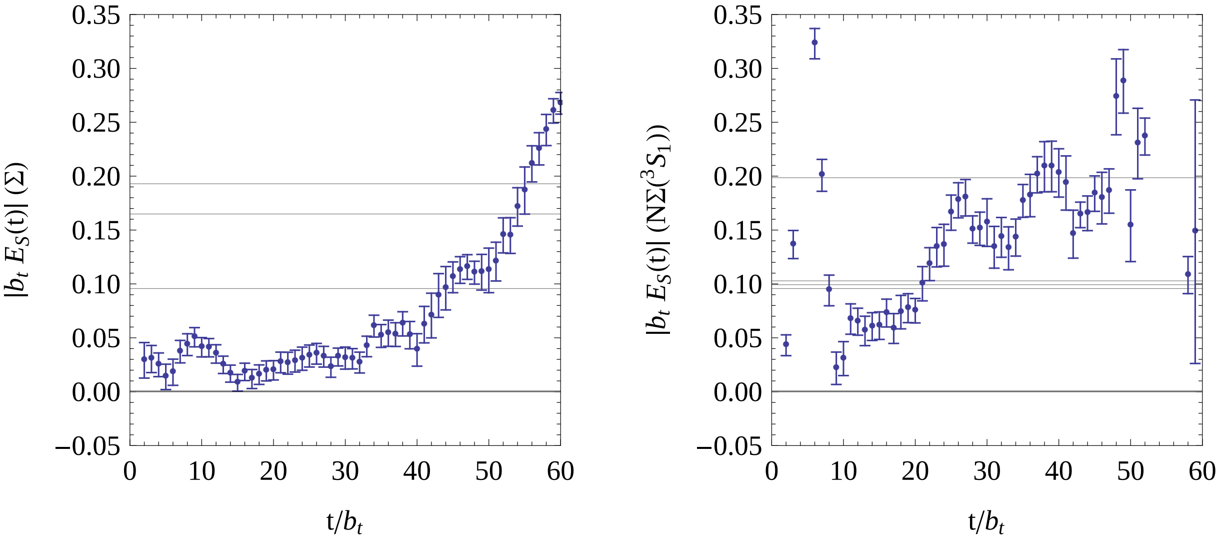

FIG. 23: The energy scale of the signal-to-noise ratio in the Σ (left panel) and the $n\Sigma^-$ $(^3S_1)$ (right panel) correlation functions, as defined in eq. (18), with $t_J = 6$. The horizontal lines in the left panel correspond to $E_s = 0$, $M_\Sigma - m_K - \frac{1}{2}m_\pi$, $M_\Sigma - m_K + \frac{1}{2}m_\pi$ and $M_\Sigma - m_\pi$, while those in the right panel correspond to $E_s = 0$, $M_N - \frac{3}{2}m_\pi$, $M_\Sigma - m_K - \frac{1}{2}m_\pi$, $\frac{1}{2}M_N + \frac{1}{2}M_\Sigma - \frac{1}{2}m_K - m_\pi$ and $M_N + M_\Sigma - m_K - 2m_\pi$.

nucleons, and serves to extend the Golden Window beyond its range in nucleon correlation functions.

E. Scaling of correlation functions, energy levels and scattering phase shifts

In generating the 0.435×10^6 measurements on this ensemble of gauge-field configurations, we have performed an average of 364 measurements on each of the 1195 configurations. The scaling of the statistical and (fitting) systematic uncertainties in the single-hadron masses as a function of the number of measurements and number of gauge-field configurations in this ensemble was detailed in Ref. [22]. While the pion mass extraction was found to saturate as the number of measurements per configuration increased, the single baryon mass extractions did not saturate and scaled in a way that is approximately consistent with each measurement on the configuration being statistically independent. It is important to determine the scaling of uncertainties associated with scattering parameters determined in this lattice QCD calculation because this scaling dictates the distribution of computational resources between the production of gauge-field configurations and the measurements performed per configuration. The $\Lambda\Lambda$ channel provides a clean illustration of the scaling that is observed in the two-baryon sector. The fit to the blue circles in fig. 27 shows the scaling of the statistical uncertainty of the extracted value of q_0^2 from the lowest level in the $\Lambda\Lambda$ correlation function. The points correspond to the inverse of the variance of q_0^2 as a function of the number of sources per configuration, $N_{\rm src}$, on 1155 gauge field configurations. The straight line corresponds to the

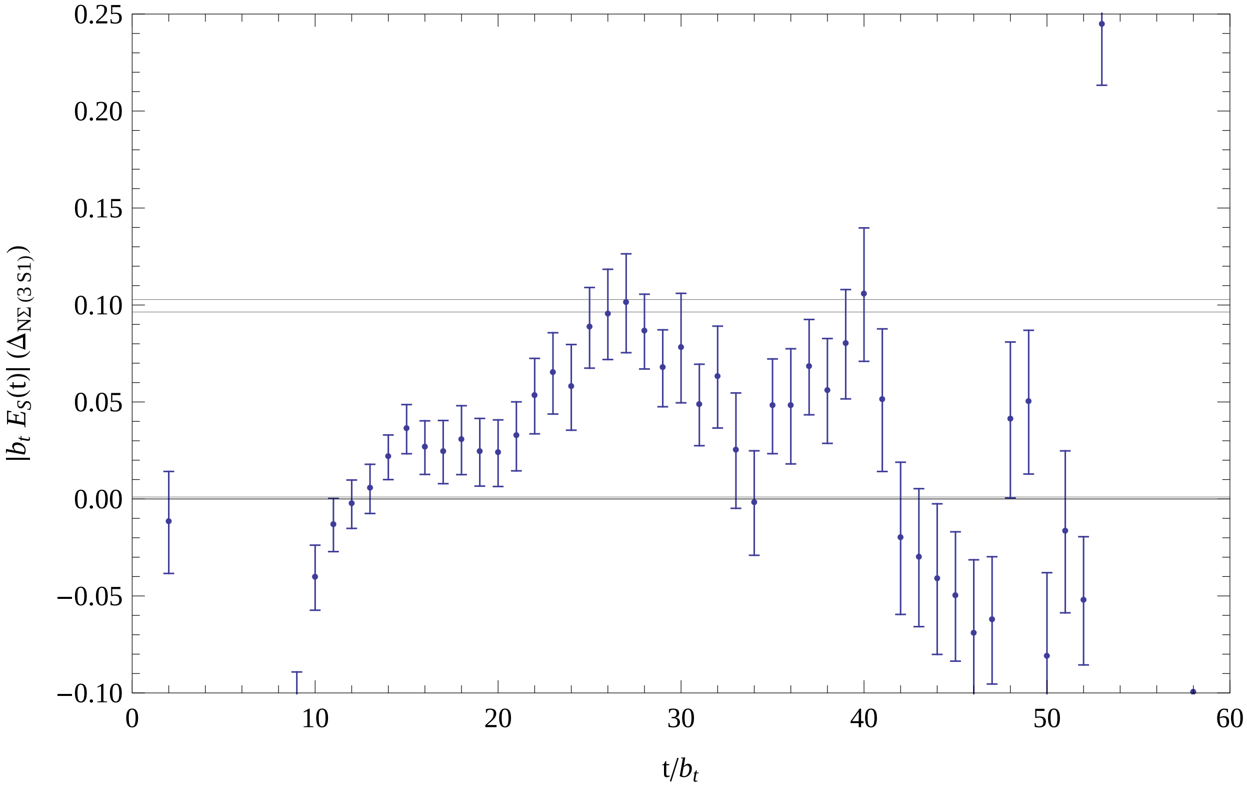

FIG. 24: The energy scale of the signal-to-noise ratio, as defined in eq. (18), in the ratio of correlation functions that produces the shift in energy between interacting Σ's and neutrons in the $^3S_1$-channel and isolated Σ's and neutrons, with $t_J = 6$. The horizontal lines correspond to $E_s = 0$, $M_N - \frac{3}{2}m_\pi$ and $M_\Sigma - m_K - \frac{1}{2}m_\pi$.

fit $1/\sigma^2 = A\ N_{\rm src}^{\alpha}$, with $\alpha = 0.94 \pm 0.04$. The fit to the purple squares in fig. 27 shows the scaling of the statistical and fitting-systematic uncertainties of the extracted value of q_0^2 from the lowest level in the ΛΛ correlation function combined in quadrature. The straight line fit gives $\alpha = 1.11 \pm 0.02$. It is clear that both the statistical, and the combined statistical and systematic uncertainties, are scaling as $\sim 1/\sqrt{N_{\rm src}}$, consistent with statistically independent measurements even up to approximately 400 measurements per configuration.

To emphasize the impact of the uncertainties on the extracted scattering parameters, and in particular, the need for high-statistics measurements of the scattering processes, fig. 28 shows the extracted values of $(p\cot\delta)^{-1}$ for ΛΛ scattering versus the extracted value of $|\mathbf{k}|^2$ for different numbers of measurements per configuration, each with 1155 gauge-field configurations. With just 10 measurements per configuration the uncertainty in $p\cot\delta$ is large enough so that it is not possible to determine if the interaction is attractive or repulsive. This remains the case even for 100 measurements per configuration. It is only when the number of measurements per configuration approaches $\sim$ 400 that the interaction can be determined to be attractive, but only with $\sim 2\sigma$ significance.

Within uncertainties, the same scaling behavior is observed in all of the two-baryon channels. It appears that further measurements could be performed on this ensemble of gauge-field configurations that would continue to reduce the uncertainties in the two-baryon correlation functions. This statement is also valid for the single-baryon correlation functions

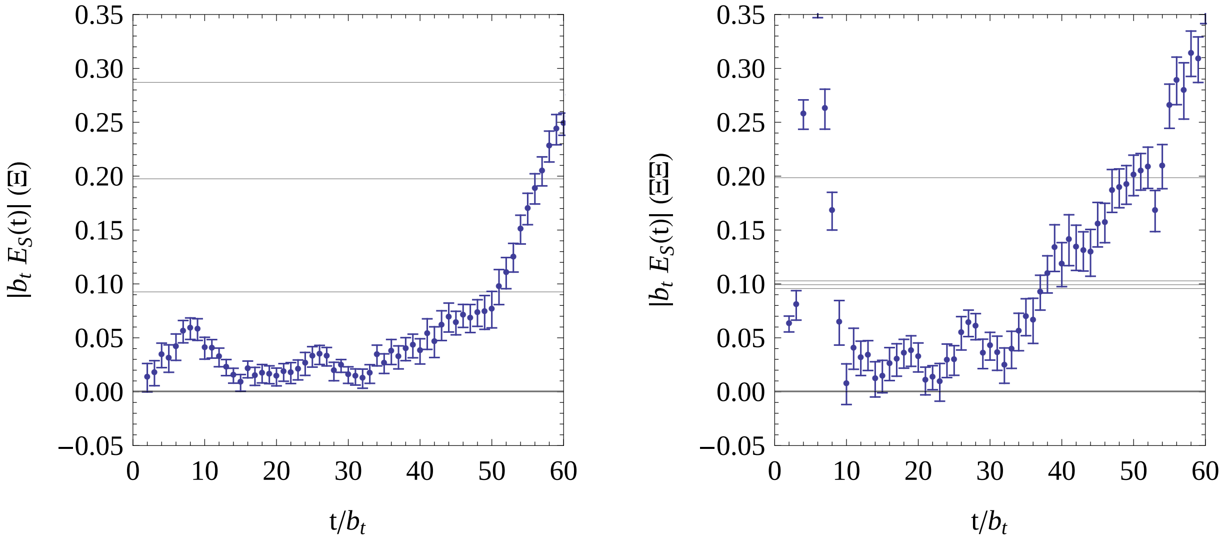

FIG. 25: The energy scale of the signal-to-noise ratio in the Ξ (left panel) and $\Xi^-\Xi^-$ (right panel) correlation functions, as defined in eq. (18), with $t_J = 6$. The horizontal lines in the left panel correspond to $E_s = 0$, $M_\Xi - m_K - \frac{1}{2}m_\eta$, $M_\Xi - m_K + \frac{1}{2}m_\eta$ and $M_\Xi + m_K - \frac{1}{2}m_\eta$, while those in the right panel correspond to $E_s = 0$, $M_\Xi - m_K - \frac{1}{2}m_\eta$, $M_\Xi - m_K + \frac{1}{2}m_\eta$, $M_\Xi + m_K - \frac{1}{2}m_\eta$ and $2(M_\Xi - m_K - \frac{1}{2}m_\eta)$.

which do not show signs of saturation.

VI. DISCUSSION

We have calculated nucleon-nucleon, hyperon-nucleon and hyperon-hyperon interactions, with a high-statistics lattice QCD calculation on anisotropic improved-clover gauge-field configurations at a pion mass of $m_\pi \sim 390$ MeV. A summary of the scattering information that has been extracted from the measurements is presented in fig. 29 and in fig. 30.

The phase shifts that we have obtained in the NN sector are small, and essentially consistent with zero. As a result we have been able to set a tight limit on the scattering lengths in both the ${}^3S_1$ and ${}^1S_0$ channels (without extrapolation in $|\mathbf{k}|^2$), as shown in fig. 6. These limits are consistent with our previous calculations of the scattering lengths in these channels [19], but significantly more precise.

Precise measurements in the YN sector (strangeness = −1) have been obtained. The interaction in the $n\Sigma^-$ (${}^3S_1$) channel is found to be strong, but we are unable to determine if the interaction is attractive or repulsive until further measurements in different lattice volumes are performed. Such calculations are in progress. The measured momentum is far outside of the region for which an effective range expansion is convergent ($|\mathbf{k}| < m_\pi/2$), and consequently arguments concerning the naturalness or unnaturalness of the scattering amplitude are not possible. In contrast, the measured momentum in the $n\Sigma^-$ (${}^1S_0$) channel is within the region for which an effective-range expansion is convergent and the scattering length and effective range are either of natural size, or there are strong cancellations in the

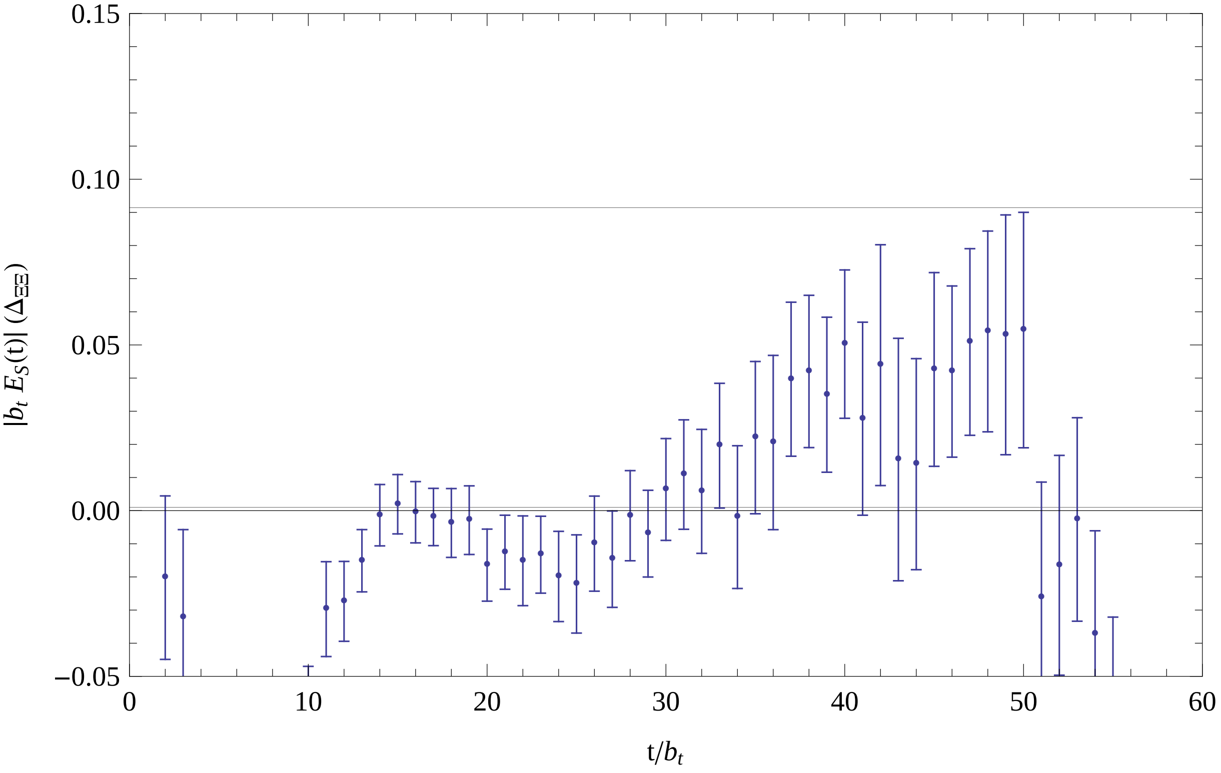

FIG. 26: The energy scale of the signal-to-noise ratio, as defined in eq. (18), in the ratio of correlation functions that produces the shift in energy between interacting Ξ^-'s and isolated Ξ's, with $t_J = 6$. The horizontal lines correspond to $E_s = 0$ and $M_\Xi - m_K - \frac{1}{2}m_\eta$.

effective range expansion. It is clear that the $n\Sigma^-$ interactions are strongly spin dependent, as is expected from the long-distance contribution from one-pion exchange. On the other hand, the ${}^1S_0$ and ${}^3S_1$ $n\Lambda$ energy shifts are very similar, and as such we conclude that the interactions are essentially spin independent, as would be expected from channels without one-pion exchange.

The measurement of a negatively-shifted energy level in the $\Lambda\Lambda$ channel (strangeness $= -2$) indicates (at the statistical precision of the measurement) that the $\Lambda\Lambda$ interaction is attractive. This is the only baryon-baryon channel for which we have measured a negative energy shift. This is an exciting measurement as it confirms that the channel in which the H-dibaryon [35] would arise is attractive. The present measurement suggest that the state does not correspond to a bound state in the infinite-volume limit at this pion mass ($m_\pi \sim 390$ MeV), but one can readily imagine that a bound state could arise at a lighter pion mass.

The present work clearly demonstrates that, with sufficient computational resources, lattice QCD can be used to extract baryon-baryon scattering amplitudes as a function of momentum, and hence constrain the interactions between baryons. As has been discussed extensively in the literature [8, 27], it is not possible to directly extract the hadron-hadron potential (unless one or more of the quarks in each hadron is infinitely heavy), but effective interactions that reproduce the measured scattering amplitudes can be constructed and used in the calculation of other quantities of interest, in the same way that the modern NN

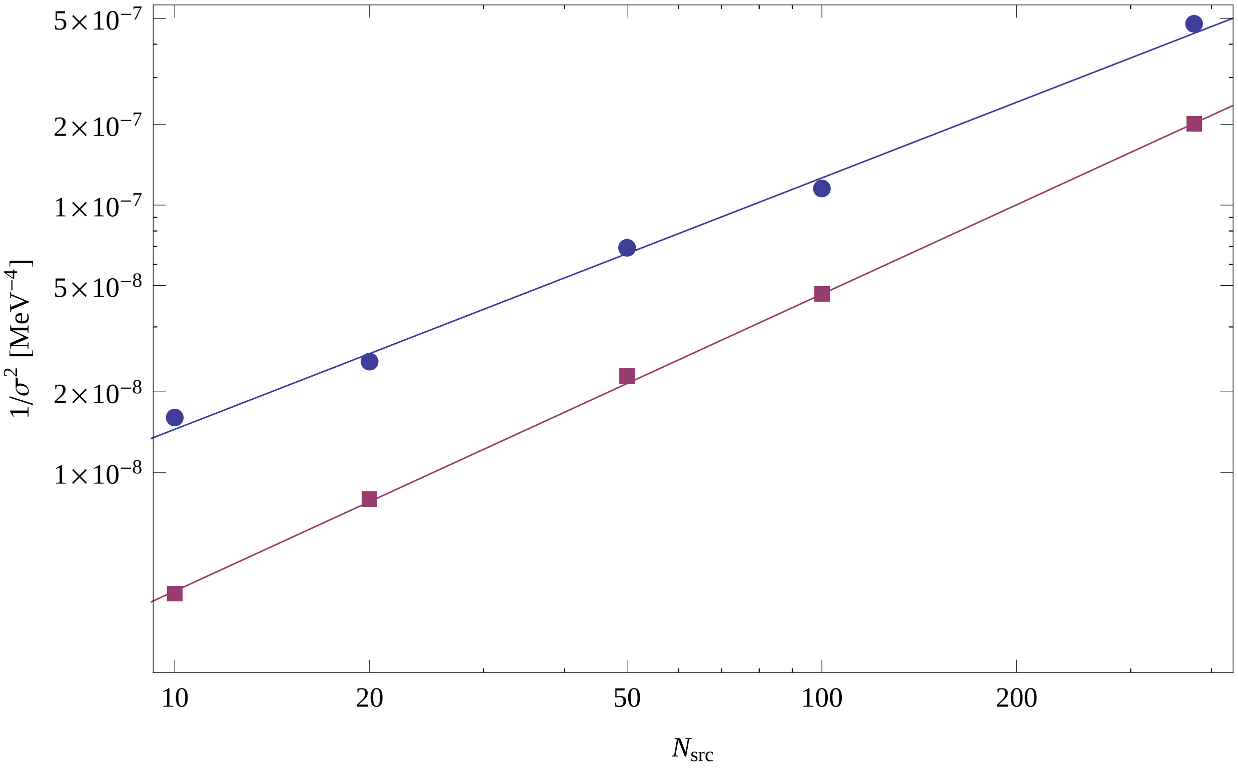

FIG. 27: The scaling of the statistical uncertainty (blue circles), and the statistical and fitting systematic uncertainties combined in quadrature (purple squares), of the extracted value of q_0^2, defined in eq. (6), for the $\Lambda\Lambda$ system as a function of the number of measurements per configuration. The vertical axis is in units of $1/\mathrm{MeV}^4$.

potentials are constructed to reproduce the experimentally-measured NN scattering cross-sections.

The detailed exploration of the behavior of the signal-to-noise ratio in the baryon-baryon correlation functions, made possible by the very large number of measurements that have been performed, has been exceptionally illuminating. The importance of the "Golden Window" of time-slices in which the signal-to-noise ratio is essentially independent of time cannot be overstated. This window allows for precise determinations of the energy-splitting between interacting baryons and isolated baryons, and in this window, the signal-to-noise ratio does not scale with baryon number, making precise measurements in multi-baryon systems feasible as discussed in Ref. [23].

This calculation is the first part of a thorough analysis of baryon-baryon scattering at this pion mass. Calculations in lattice volumes that are both larger and smaller than the present lattice volume are underway and will provide measurements of the scattering amplitude at two additional momenta. In most channels, this will allow for a determination of the scattering parameters (scattering lengths and effective-range parameters) at this pion mass. However, it is important to keep in mind that all of these measurements will be at a single lattice spacing, $b_s \sim 0.123$ fm. In order to make precise statements, even at this larger pion mass, measurements at smaller lattice spacings will be required.

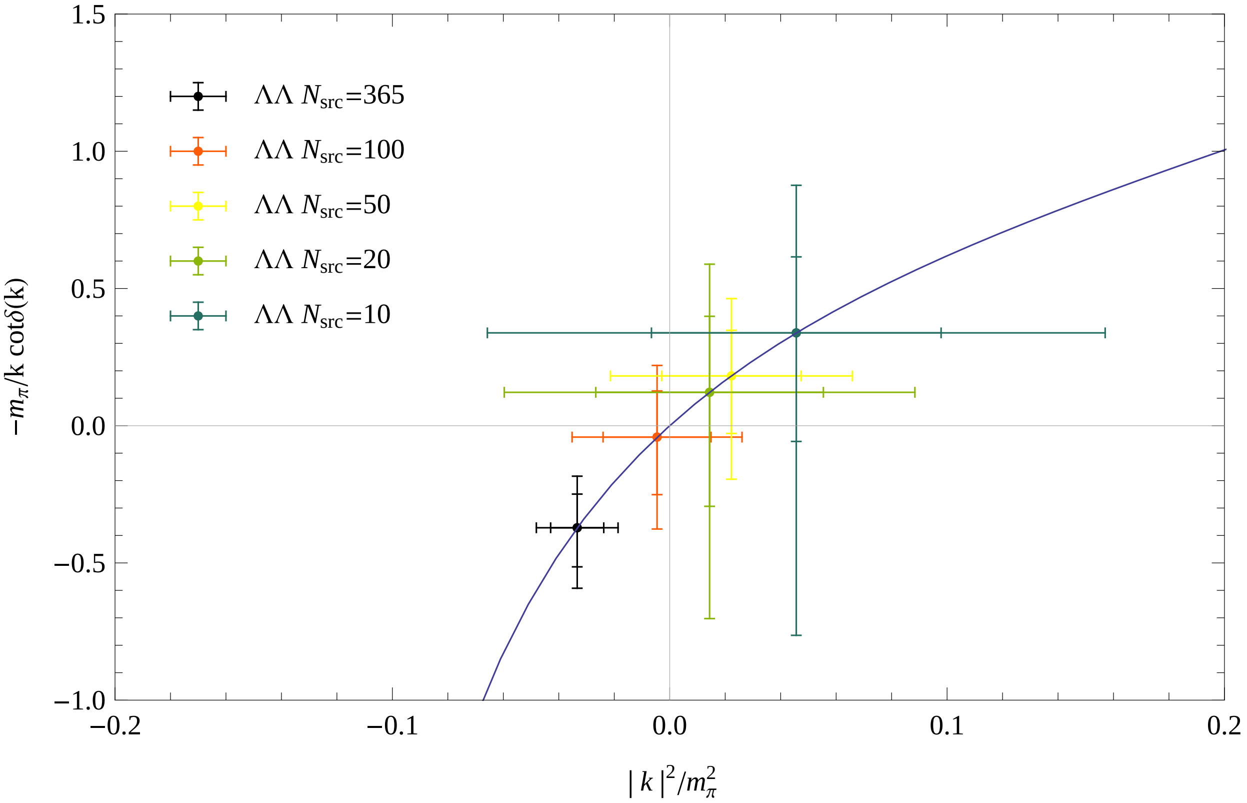

FIG. 28: The extracted values of the inverse of the real part of the inverse of the ΛΛ scattering amplitude versus the extracted value of $|\mathbf{k}|^2$, defined in eq. (6). The measured values correspond to different numbers of measurements per configuration.

VII. ACKNOWLEDGMENTS

We thank Assumpta Parreño for numerous discussions. We thank R. Edwards and B. Joo for help with the QDP++/Chroma programming environment [36]. KO thanks A Stathopoulos for collaboration in developing the EigCG algorithm used in this work [37]. We also thank the Hadron Spectrum Collaboration for the use of the anisotropic gauge-field configurations, and extending the particular ensemble used herein. We gratefully acknowledge the computational time provided by NERSC (Office of Science of the U.S. Department of Energy, No. DE-AC02-05CH11231), the Institute for Nuclear Theory, Centro Nacional de Supercomputación (Barcelona, Spain), Lawrence Livermore National Laboratory, and the National Science Foundation through Teragrid resources provided by the Texas Advanced Computing Center. Computational support at Thomas Jefferson National Accelerator Facility and Fermi National Accelerator Laboratory was provided by the USQCD collaboration under *The Secret Life of a Quark*, a U.S. Department of Energy SciDAC project (`http://www.scidac.gov/physics/quarks.html`). AT acknowledges the kind hospitality of the NCSA. The work of MJS and H-WL was supported in part by the U.S. Dept. of Energy under Grant No. DE-FG03-97ER4014. The work of KO and WD was supported in part by the U.S. Dept. of Energy contract No. DE-AC05-06OR23177 (JSA) and DOE grant DE-FG02-04ER41302. KO was also supported by NSF grant CCF-0728915. KO and AWL were supported in part by the Jeffress Memorial Trust, grant J-813 and DOE OJI

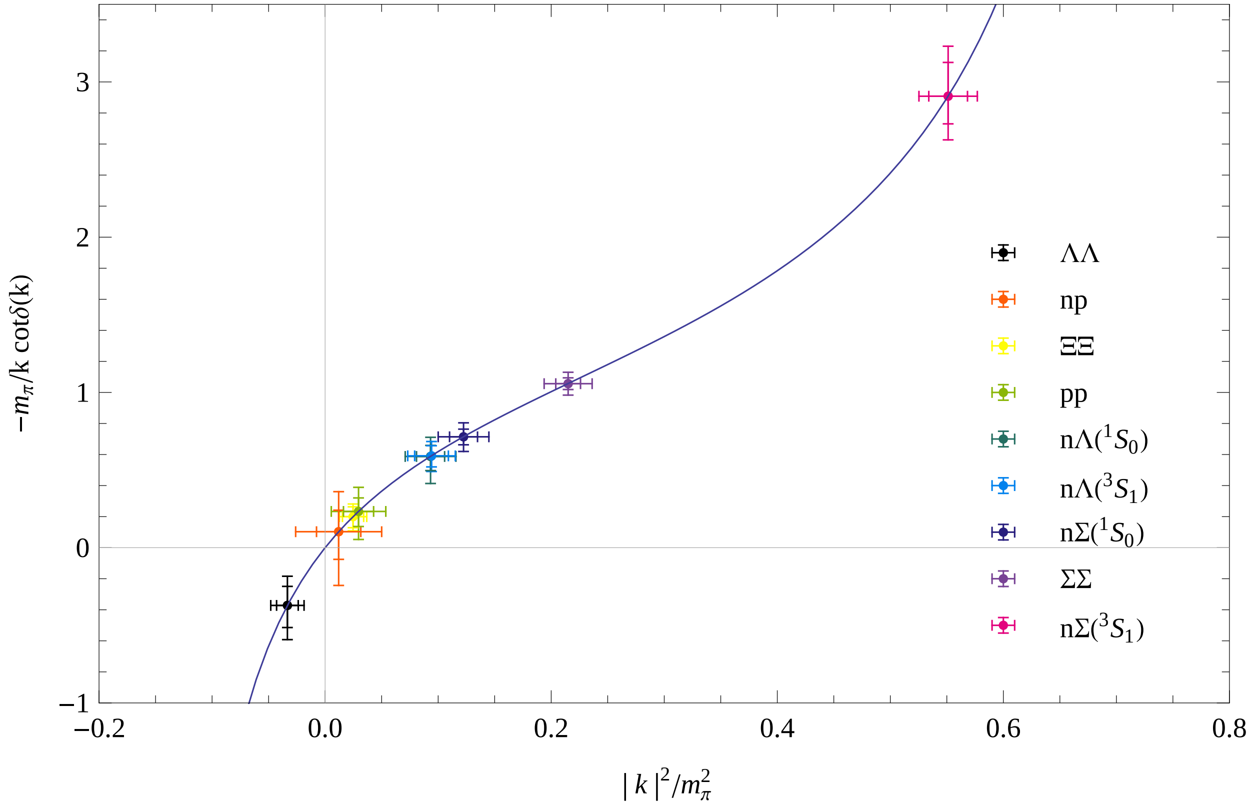

FIG. 29: A summary of the baryon-baryon scattering information measured in this work. The top-most point of the plot-legend corresponds to the left-most point on the plot, and the bottom-most point of the plot-legend corresponds to the right-most point on the plot. The other points are ordered accordingly.

grant DE-FG02-07ER41527. WD was also supported by DOE OJI grant de-sc0001784. The work of SRB was supported in part by the National Science Foundation CAREER grant No. PHY-0645570. The work of AT is currently supported by NSF Grant PHY-0555234 and DOE grant DE-FC02-06ER41443. Part of this work was performed under the auspices of the US DOE by the University of California, Lawrence Livermore National Laboratory under Contract No. W-7405-Eng-48.

---

[1] `http://nn-online.org/`

[2] R. B. Wiringa, V. G. J. Stoks and R. Schiavilla, Phys. Rev. C **51**, 38 (1995) [arXiv:nucl-th/9408016].

[3] E. Epelbaum, H. W. Hammer and U. G. Meissner, arXiv:0811.1338 [nucl-th].

[4] S. C. Pieper, Riv. Nuovo Cim. **031**, 709 (2008) [arXiv:0711.1500 [nucl-th]].

[5] S. C. Pieper, R. B. Wiringa and J. Carlson, Phys. Rev. C **70**, 054325 (2004) [arXiv:nucl-th/0409012].

[6] P. Navratil, V. G. Gueorguiev, J. P. Vary, W. E. Ormand and A. Nogga, Phys. Rev. Lett. **99**, 042501 (2007) [arXiv:nucl-th/0701038].

[7] D. Page and S. Reddy, Ann. Rev. Nucl. Part. Sci. **56**, 327 (2006) [arXiv:astro-ph/0608360].

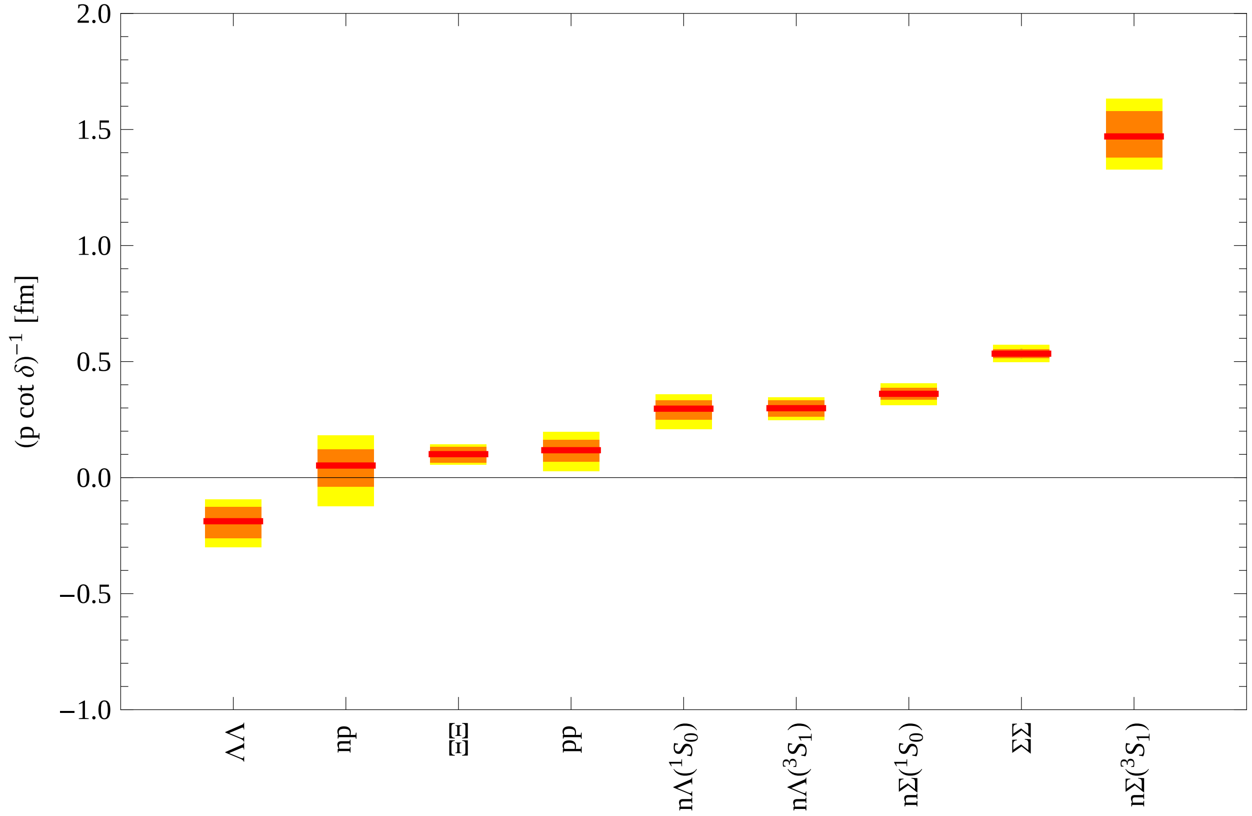

FIG. 30: The inverse of the real part of the inverse scattering amplitude for all of the baryon-baryon scattering channels calculated in this work. Each is determined at a different value of the two-baryon center-of-mass energy.

[8] S. R. Beane, K. Orginos and M. J. Savage, Int. J. Mod. Phys. E **17**, 1157 (2008) [arXiv:0805.4629 [hep-lat]].

[9] S. R. Beane, P. F. Bedaque, K. Orginos and M. J. Savage [NPLQCD Collaboration], Phys. Rev. D **73**, 054503 (2006) [arXiv:hep-lat/0506013].

[10] S. R. Beane, T. C. Luu, K. Orginos, A. Parreno, M. J. Savage, A. Torok and A. Walker-Loud, Phys. Rev. D **77**, 014505 (2008) [arXiv:0706.3026 [hep-lat]].

[11] X. Feng, K. Jansen and D. B. Renner, arXiv:0909.3255 [hep-lat].

[12] S. R. Beane, W. Detmold, T. C. Luu, K. Orginos, M. J. Savage and A. Torok, Phys. Rev. Lett. **100**, 082004 (2008) [arXiv:0710.1827 [hep-lat]].

[13] W. Detmold, M. J. Savage, A. Torok, S. R. Beane, T. C. Luu, K. Orginos and A. Parreno, Phys. Rev. D **78**, 014507 (2008) [arXiv:0803.2728 [hep-lat]].

[14] W. Detmold, K. Orginos, M. J. Savage and A. Walker-Loud, Phys. Rev. D **78**, 054514 (2008) [arXiv:0807.1856 [hep-lat]].

[15] H. W. Hamber, E. Marinari, G. Parisi and C. Rebbi, Nucl. Phys. B **225**, 475 (1983).

[16] M. Lüscher, Commun. Math. Phys. **105**, 153 (1986).

[17] M. Lüscher, Nucl. Phys. B **354**, 531 (1991).

[18] G. P. Lepage, ‘The Analysis Of Algorithms For Lattice Field Theory,” Invited lectures given at

TASI'89 Summer School, Boulder, CO, Jun 4-30, 1989. Published in Boulder ASI 1989:97-120 (QCD161:T45:1989).

[19] S. R. Beane, P. F. Bedaque, K. Orginos and M. J. Savage [NPLQCD Collaboration], Phys. Rev. Lett. **97**, 012001 (2006) [arXiv:hep-lat/0602010].

[20] S. R. Beane, P. F. Bedaque, T. C. Luu, K. Orginos, E. Pallante, A. Parreno and M. J. Savage [NPLQCD Collaboration], Nucl. Phys. A **794**, 62 (2007) [arXiv:hep-lat/0612026].

[21] A. Torok *et al.*, arXiv:0907.1913 [hep-lat].

[22] S. R. Beane *et al.*, Phys. Rev. D **79**, 114502 (2009) [arXiv:0903.2990 [hep-lat]].

[23] S. R. Beane *et al.*, Phys. Rev. D **80**, 074501 (2009) [arXiv:0905.0466 [hep-lat]].

[24] R. G. Edwards, B. Joo and H. W. Lin, Phys. Rev. D **78**, 054501 (2008) [arXiv:0803.3960 [hep-lat]].

[25] H. W. Lin *et al.* [Hadron Spectrum Collaboration], Phys. Rev. D **79**, 034502 (2009) [arXiv:0810.3588 [hep-lat]].

[26] T. Yamazaki, Y. Kuramashi, A. Ukawa, arXiv:0912.1383 [hep-lat].

[27] W. Detmold, K. Orginos and M. J. Savage, Phys. Rev. D **76**, 114503 (2007) [arXiv:hep-lat/0703009].

[28] M. Fukugita, Y. Kuramashi, M. Okawa, H. Mino and A. Ukawa, Phys. Rev. D **52**, 3003 (1995) [arXiv:hep-lat/9501024].

[29] S. Aoki, T. Hatsuda and N. Ishii, Comput. Sci. Dis. **1**, 015009 (2008) [arXiv:0805.2462 [hep-ph]].

[30] S. R. Beane and M. J. Savage, Nucl. Phys. A **713**, 148 (2003) [arXiv:hep-ph/0206113].

[31] S. R. Beane and M. J. Savage, Nucl. Phys. A **717**, 91 (2003) [arXiv:nucl-th/0208021].

[32] E. Epelbaum, U. G. Meissner and W. Gloeckle, Nucl. Phys. A **714**, 535 (2003) [arXiv:nucl-th/0207089].

[33] H. Nemura, N. Ishii, S. Aoki and T. Hatsuda [PACS-CS Collaboration], arXiv:0902.1251 [hep-lat].

[34] H. Nemura, N. Ishii, S. Aoki and T. Hatsuda, Phys. Lett. B **673**, 136 (2009) [arXiv:0806.1094 [nucl-th]].

[35] R. L. Jaffe, Phys. Rev. Lett. **38**, 195 (1977) [Erratum-ibid. **38**, 617 (1977)].

[36] R. G. Edwards and B. Joo [SciDAC Collaboration], Nucl. Phys. Proc. Suppl. **140** (2005) 832 [arXiv:hep-lat/0409003].

[37] A. Stathopoulos and K. Orginos, arXiv:0707.0131 [hep-lat].